Hindawi
International Journal of Aerospace Engineering
Volume 2021, Article ID 5522379, 28 pages
https://doi.org/10.1155/2021/5522379

Research Article

Robust Finite-Time Trajectory Tracking Control of Quadrotor Aircraft via Terminal Sliding Mode-Based Active Antidisturbance Approach: A PIL Experiment

Omar Mechali,[1,2] Jamshed Iqbal,[3] Xiaomei Xie ,[1,2] Limei Xu,[1,2] and Abdelkader Senouci[4]

[1]*School of Aeronautics and Astronautics, University of Electronic Science and Technology of China, Chengdu 611731, China*
[2]*Aircraft Swarm Intelligent Sensing and Cooperative Control Key Laboratory of Sichuan Province, University of Electronic Science and Technology of China, Chengdu 611731, China*
[3]*Department of Computer Science and Technology, Faculty of Science and Engineering, University of Hull, HU6 7RX, UK*
[4]*Faculty of Engineering and Environment, Northumbria University, Newcastle upon Tyne, UK*

Correspondence should be addressed to Xiaomei Xie; mayxiezhou@uestc.edu.cn

Received 30 January 2021; Revised 30 March 2021; Accepted 16 April 2021; Published 6 May 2021

Academic Editor: Erkan Kayacan

This paper presents an accurate solution of finite-time Cartesian trajectory tracking control problem of a quadrotor system by designing and implementing a novel robust flight-control algorithm. The quadrotor is subject to nonlinearities, unmodeled dynamics, parameters' uncertainties, and external time-varying disturbances. To reject the disturbances and enhance the control system's robustness, a terminal sliding mode-based active antidisturbance control (TSMBAADC) approach is proposed for rotational and translational subsystems. To improve the tracking performance, a nonlinear continuous terminal sliding manifold and a fast reaching law are proposed in this work to quickly drive the systems' states to the equilibrium point even in the presence of lumped disturbances. The convergence time of the states can be pretuned based on the parameters of the sliding manifold and the reaching law. Lyapunov theorem is used to provide a rigorous stability proof for the feedback control system. Numerical simulations and processor-in-the-loop (PIL) experiments are conducted to validate and implement the designed flight control algorithm on real autopilot hardware. The novelty of the proposed research lies in hardware implementation of a sophisticated version of modern control technique that exhibits a multitude of distinguishing features including but not limited to (i) finite-time tracking stability featuring fast convergence is ensured, (ii) chattering and singularity problems in sliding mode control (SMC) are avoided, and (iii) null steady-state error is achieved along with enhanced robustness. Finally, the proposed control law is compared with two recently reported research works. Results of performance comparison in term of the integral of square error (ISE) and the absolute value of the derivative of the input $u(t)$ (IADU) dictate that the proposed technique overperforms by precision and chattering alleviation.

1. Introduction

1.1. Context and Motivations. Nowadays, quadrotor aircraft have gained enormous interest due to their numerous merits such as low-cost manufacturability and vertical take-off and landing capability [1–3]. These interesting aircraft have been widely used in many fields to solve practical and complex missions [4–8]. However, despite their advantages, quadrotors have some critical drawbacks that are related to flight control. The quadrotor is a nonlinear multioutput multi-input system with underactuated six degrees of freedom (6-DoF) dynamics [9]. Moreover, the quadrotor's dynamics are strongly coupled and inevitably affected by multiple disturbances [10, 11]. Meanwhile, the quadrotor is intended to operate in a challenging flight environment where it may perform aggressive maneuvers. Thus, its stabilization and control in such flight conditions is not trivial but a challenging and complex task. The robust trajectory tracking control during flight missions is one of the persistent control problems. This problem has become an important topic that should

be carefully addressed by the control community. Particularly, fast convergence, strong robustness, and accuracy are considered important features of a flight control algorithm to safely and effectively drive the quadrotor during the mission. Therefore, a reliable flight control system essentially relying on a modern control technique is required to achieve good tracking performance. Hence, this paper focuses on the design of a new flight-control system to deal with the robust Cartesian trajectory tracking control problem for the quadrotor system.

1.2. Literature Review and Contributions. Recently, a large and growing body of literature has been focused on the Cartesian trajectory tracking control problem of the quadrotor system using finite-time control, as stated in [12, 13]. In contrast to classical asymptotically stable controllers, finite-time stable control systems ensure fast convergence of the system's trajectories to the origin along with higher accuracy and enhanced robustness. Motivated by the mentioned works, the finite-time tracking control problem for the quadrotor system is investigated in this study.

Multiple works have been reported on the trajectory tracking control problem of the quadrotor helicopter. Linear control such as proportional-integral-derivative (PID) [14–16] and linear quadratic regulator (LQR) [17, 18] have been initially used to design flight control systems for the quadrotor. However, linear control can only ensure good performance around a specific equilibrium point of the linearized model of the quadrotor. In practice, the quadrotor is intended to operate in a challenging flight environment and may exhibit aggressive maneuvers leading to strong nonlinear behavior. Therefore, the linear control seems to be unable to ensure the required flight performance during the mission. Hence, to design an adequate flight control system that can ensure a safe flight for the quadrotor, nonlinear control is considered a reliable tool that can overcome the shortcoming of classical linear control.

Backstepping (BS) is Lyapunov's theory-based recursive and flexible nonlinear control design methodology that can be used to deal with the control problem of high-order nonlinear systems such as the quadrotor aircraft [19]. For instance, the work reported in [20] employs a nonlinear adaptive BS method for a trajectory tracking control of the quadrotor. A robust adaptive BS is designed for the position loop in [21]. However, the BS design technique suffers from three main issues: the "explosion of complexity", lack of robustness against disturbances, and only asymptotic stability in infinite-time is guaranteed, as reported in [22, 23]. Unfortunately, many reported works, e.g., [21, 24] do not address these issues. In practice, the implementation of a control law with such issues could lead to system instability and mission failure. The present research is aimed at solving the problem inherently present in classical BS control design so as to further improve its performance. In particular, (a) a sliding-mode-based filter (SMBF) is introduced in the recursive BS design to restore the derivative of the virtual control to avoid the "explosion of complexity" problem. (b) Terminal sliding mode control (TSMC) is combined with the BS technique to ensure finite-time stability featuring fast transient response. (c) A disturbance observer is designed to enhance the disturbance rejection capability of the compounded controller.

SMC control has been effectively applied for control design and stabilization of a variety of nonlinear dynamical systems such as the underactuated quadrotor system. This is motivated by its robustness against uncertainties and disturbances and simplicity of control design [25–28]. The design procedure of the SMC control systems mainly consists of two steps: the choice of a sliding surface with desirable dynamic characteristics and the design of the SMC controller. The controller is designed such that the system's states reach and remain on the sliding manifold and consequently converge to the origin. Recently, many works are concerned with the robust control of the quadrotor system subjected to disturbances using SMC theory. As an example of sliding mode combination with BS, the work in [29] presents an integral backstepping sliding mode control (IBSMC) method for a perturbated quadrotor system. In [30], a regular SMC is combined with the BS technique to design a robust nonlinear controller. Nevertheless, all these methods are based on linear sliding mode control (LSMC). The most serious disadvantage of this control approach is that the switching manifold is linear. Thus, only asymptotic convergence can be achieved. Also, LSMC inevitably suffers from the chattering problem. The chattering impact is reflected by the presence of disrupting high switching frequencies in the control input of the system [31]. Such a control signal will cause low control accuracy and degrade the control performance [26]. Furthermore, it can also damage the actuators of the quadrotor (the brushless motors). To deal with the issues of LSMC, this study proposes to use advanced continuous-SMC techniques. The proposed terminal sliding manifold in our work allows that tracking errors are stabilized to the origin in fast finite-time by contrast to the linear switching manifold that can only guarantee asymptotic convergence in an infinite time. Moreover, the control law designed based on our terminal sliding surface is continuous; hence, the chattering problem inherent in SMC and switching control methods can be effectively mitigated, which makes the controller applicable in practice.

In order to ensure better tracking control performance, finite-time control is considered in many works. For instance, in the interesting work [32], Mobayen and Ma have innovatively proposed a robust finite-time composite nonlinear feedback control for synchronization of uncertain chaotic systems with nonlinearity and time delay. The same authors have investigated a novel nonsingular fast terminal sliding-mode control method for the stabilization of the uncertain time-varying and nonlinear third-order systems in [25]. A recursive singularity-free fast terminal sliding mode control is used in [33] to design a finite-time tracker for nonholonomic systems including a wheeled mobile robot and an underactuated surface vessel. In [34], by designing an LMI-based sliding mode controller, the state trajectories of a class of underactuated systems are shown to be directed toward the sliding manifold in a finite-time with exponential policy and thereafter remained on it. Although the above studies have interesting and promising results from theoretical and

practical aspects, they have not been applied specifically to solve the trajectory tracking problem quadrotor system, which motivates us to further investigate the finite-time control of quadrotor aircraft.

In our recently published study [27], a finite-time observer-based robust continuous twisting control is proposed for an uncertain quadrotor system subjected to disturbances. Another work reported in [35] comes up with a modified super twisting algorithm that can ensure robustness and finite-time convergence for the quadrotor helicopter. In the work [36], the tracking errors are driven to zero in finite-time by employing a fractional-order controller based on nonsingular control law. However, these studies are limited to the finite-time control of the 3-DoF attitude dynamics, and they did not address the finite-time control of the full 6-DoF dynamics of the quadrotor. Also, the attitude dynamics are fully actuated with three inputs and three outputs which makes the control design much easier. Our study includes finite-time control for the 6-DoF dynamics, i.e., attitude and position subsystems, where the underactuated problem inherent in the quadrotor dynamics has been addressed.

To address the finite-time control of attitude and position of the quadrotor, a modified super twisting fast nonlinear sliding mode controller is proposed to stabilize a quadrotor system under time-varying disturbances in [37], in finite-time. Also, a finite-time trajectory tracking control for a quadrotor aircraft with unknown external disturbances is investigated in [38]. However, together with [21], the works [37, 38] have presented the design of the control laws by considering a perfect model with precise knowledge of the model parameters. In practice, it is difficult to identify and estimate the exact parameters of the quadrotor system, notably, the aerodynamic coefficients. Besides, model uncertainties are inevitably present in the dynamic model of the quadrotor. Therefore, unlike these works, model uncertainties are also considered in our study besides external time-varying disturbances, which is more realistic in practice. Some reported works on finite-time control have considered the model imperfection and uncertainties in the control design; however, they have not provided an upper bound on the settling-time, e.g., [37, 39]. It is well-known that one of the most interesting features of finite-time stability is that an upper bound on the settling-time can be provided and tuned in the function of the control parameters. Therefore, in contrast to [37, 39], we have established a clear estimation of the settling-time during the sliding motion which allows tuning the convergence-time by adjusting the parameters of the sliding surface and the reaching law.

In [40], a nonsingular terminal sliding mode control law with finite-time convergence is designed for the quadrotor. In [41], a finite-time convergent nonsingular terminal sliding mode control for a quadrotor with a total rotor failure is proposed. In [42], finite-time adaptive integral backstepping fast terminal sliding mode control is applied for the tracking of the attitude and position of the quadrotor. Although [21, 40–42] provide an estimation of the settling-time, the sign $(\cdot)$ function appears explicitly in the control law, which may cause the chattering and thus making the controller inapplicable in practice. To reduce the chattering effect, the authors have replaced the sign $(\cdot)$ function with smooth approximating functions. However, this may degrade the robustness of the controller leading to a chattering-robustness tradeoff. By contrast to that, no smooth functions are required to approximate the sign $(\cdot)$ function in our control law. Hence, the robustness of the sliding mode is well preserved along with a chattering-free control.

Overall, the abovementioned finite-time control methods are limited in terms of performance and their application since full-state measurements are required. The signals provided by the gyroscope and accelerometer sensors for the velocity measurement are affected by noise. This issue may lead to degrading the performance of full-state feedback-based controllers. Also, the sensors are exposed to faults that inevitably compromise the stability of the quadrotor leading to mission failure [43]. To deal with this practical shortcoming of full-state feedback-based finite-time controllers, we propose in our study to design an output-feedback control method (velocity-free control) that contributes to enhancing the quadrotor's robustness and in estimating the unmeasurable states (velocities) at the same time within an active disturbance rejection control (ADRC) framework. Our approach shows its effectiveness and superiority over classical passive antidisturbance control laws that fail to deal with strong disturbances leading to the degradation of the nominal control's performance which may threaten the system's stability, as mentioned in [44, 45].

Moreover, most of the reported works on finite-time control of the quadrotor aircraft may look very promising as evidenced by simulation results. However, owing to lack of practical implementation, their real-world significance may be a valid concern. In contrast, the present paper presents design, simulation, and hardware realization of modern robust finite-time control laws. The physical implementation in autopilot hardware while attempting to address the abovementioned problems essentially attributes to the scientific contribution of our work.

Motivated by the previously reported studies and inspired by the works developed in [46, 47], this paper focuses on addressing all the issues discussed above by designing a new robust flight-control system to deal with the Cartesian trajectory tracking control problem of a quadrotor system subject to lumped disturbances. To solve the underactuation problem, a hierarchical control structure with a position-attitude loop is adopted. To reject the disturbances and enhance the control system robustness, a TSMBAADC approach is employed in each loop. In this context, a disturbance observer-based control (DOBC) law is designed for the attitude loop while the position loop is controlled by an innovatively designed ADRC scheme. The compounded DOBC control structure integrates a finite-time observer (FTO) and a continuous nonsingular terminal sliding mode control (CNTSMC). In practice, it is more reliable to use the technique of differentiators in the implementation process of the control algorithm. Thus, a tracking differentiator is designed to supply the estimates of desired attitude signals. The ADRC control is designed within an output-feedback scheme to ensure a velocity-free control. It combines a fixed-time extended state

observer (FXESO) and a backstepping integral terminal sliding mode control (BSITSMC). To avoid the "explosion of complexity" problem inherent in the classic BS design, a sliding-mode-based filter (SMBF) is introduced in the recursive BS design to restore the derivative of the virtual control. By designing nonlinear continuous terminal sliding surfaces, fast finite-time convergence of the tracking errors is ensured for both rotational and translational subsystems. Lyapunov theorem is used to analyze the stability of the feedback control system. Numerical simulations and PIL experiments are conducted to validate and implement the designed flight control algorithm in real autopilot hardware. Compared with relevant reported works, the suggested control strategy has the overall superiority in practice because (i) null steady-state error is achieved along with enhanced robustness, (ii) chattering and singularity problems of SMC and switching control are avoided, and (iii) proposed sliding manifolds and reaching law allows finite-time tracking stability featuring fast convergence.

The remaining manuscript is arranged in four sections detailed here. Section 2 presents fundamentals mathematical formulation. Section 3 details the design of the proposed flight control system. Rigorous stability analysis of the feedback loop system is also discussed. Section 4 illustrates implementation results to investigate the theoretical findings. The paper is concluded in Section 5 with possible future research directions.

2. Preliminaries and Problem Formulation

This section presents some relevant mathematical definitions and lemmas employed in the control design and finite-time stability proof. The control problem of our study is also formulated in this section.

2.1. Preliminaries

Definition 1 (see [48]) (finite-time stability). Consider the following autonomous system:

$$\dot{x} = f(x), x(0) = x_0, \tag{1}$$

where $x \in \mathbb{R}^n$, and the nonlinear function $f : \mathrm{D} \to \mathbb{R}^n$ is continuous on an open neighborhood $\mathrm{D} \subseteq \mathbb{R}^n$ of the origin. The origin $x = 0$ is an equilibrium point of system (1). $x = 0$ is a globally finite-time convergent, if it is globally asymptotically stable, and there are an open neighborhood $\mathrm{U} \subseteq \mathrm{D}$ of the origin and a function $T_x : \mathrm{U} \setminus \{0\} \to (0,\infty)$ such that every solution $x(t, x_0)$ of system (1) that starts from the initial condition $x_0 \in \mathrm{U} \setminus \{0\}$ is well-defined for $t \in [0, T_x(x_0))$, and $\lim_{t \to T_x(x_0)} x(t, x_0) = 0$. Here, $T_x(x_0)$ is called the settling-time function, i.e., convergence-time, (w.r.t x_0). $x = 0$ is said to be a finite-time stable equilibrium if it is finite-time convergent and Lyapunov stable. If $\mathrm{U} = \mathrm{D} = \mathbb{R}^n$, the origin is said to be a globally finite-time stable equilibrium.

Lemma 2 (see [49]). *Consider the following system:*

$$\begin{aligned}
\dot{\sigma}_0 &= -\rho_0 L_d^{1/(n+1)} |\sigma_0|^{1/(n+1)} \operatorname{sign}(\sigma_0) + \sigma_1, \\
\dot{\sigma}_1 &= -\rho_1 L_d^{1/n} |\sigma_1 - \dot{\sigma}_0|^{(n-1)/n} \operatorname{sign}(\sigma_1 - \dot{\sigma}_0) + \sigma_2, \\
&\vdots \\
\dot{\sigma}_{n-1} &= -\rho_{n-1} L_d^{1/2} |\sigma_{n-1} - \dot{\sigma}_{n-2}|^{1/2} \operatorname{sign}(\sigma_{n-1} - \dot{\sigma}_{n-2}) + \sigma_n, \\
\dot{\sigma}_n &\in -\rho_n L_d \operatorname{sign}(\sigma_n - \dot{\sigma}_{n-1}) + [-L_d, L_d].
\end{aligned} \tag{2}$$

If the constants L_d, ρ_i satisfy $L_d > 0$ and $\rho_i > 0, i = \overline{0, n}$, it results that the above system is finite-time stable.

Lemma 3 (see [50]). *If the positive constants $k_j > 0, (j = \overline{1, n})$ make the n-order polynomials $s^n + k_n s^{n-1} + \cdots + k_2 s + k_1$ and $s^n + 3k_n s^{n-1} + \cdots + 3k_2 s + 3k_1$ be Hurwitz in terms of the Laplace operator s, i.e., all their roots are in the left-half plane, the origin of the following system*

$$\begin{cases}
\dot{x}_i = x_{i+1}, i = \overline{1, n-1}, \\
\dot{x}_n = -\sum_{j=1}^{n} k_j \left(\lceil x_j \rfloor^{\alpha_{1,j}} + \lceil x_j \rfloor + \lceil x_j \rfloor^{\alpha_{2,j}} \right),
\end{cases} \tag{3}$$

is finite-time stable equilibrium with uniform settling-time, where $\alpha_{1,j}$ and $\alpha_{2,j}$ are determined according to the bi-limit homogeneity reasoning as follows: $\alpha_{1,n-k} = \alpha/(k(1-\bar{\alpha}) + 1)$ and $\alpha_{2,n-k} = (2-\bar{\alpha})/(k(\bar{\alpha}-1) + 1)$, where $\bar{\alpha} \in (\epsilon, 1)$, $\epsilon \in (n - 2/n - 1, 1)$, and $k = \overline{0, n-1}$.

Lemma 4 (see [48]). *Suppose that there is a continuous and positive-definite Lyapunov function $V(x(t)) : \mathbb{R}^n \to \mathbb{R}$, and its derivative satisfies*

$$\dot{V}(x(t)) \le -\lambda V^{\alpha} - \mu V^{\gamma}, \tag{4}$$

where $\lambda, \mu > 0, \alpha > 1$, and $\gamma < 1$ are some positive constants, then, the origin of system (1) is fixed-time stable. The settling-time function T_0 is bounded by T^* as

$$T_0 \le T^* := \frac{1}{\lambda(\alpha - 1)} + \frac{1}{\mu(1 - \gamma)}. \tag{5}$$

Lemma 5 (see [51]). *Consider the following system:*

$$\begin{cases}
\dot{\sigma}_1 = \sigma_2 - \rho_1 \lceil \sigma_0 \rfloor^{a_1} - \bar{\rho}_1 \lceil \sigma_0 \rfloor^{b_1}, \\
\dot{\sigma}_2 = \sigma_3 - \rho_2 \lceil \sigma_0 \rfloor^{a_2} - \bar{\rho}_2 \lceil \sigma_0 \rfloor^{b_2}, \\
\quad \vdots \\
\dot{\sigma}_{n-1} = \sigma_n - \rho_{n-1} \lceil \sigma_0 \rfloor^{a_{n-1}} - \bar{\rho}_{n-1} \lceil \sigma_0 \rfloor^{b_{n-1}}, \\
\dot{\sigma}_n \in -\rho_n \lceil \sigma_0 \rfloor^{a_n} - \bar{\rho}_n \lceil \sigma_0 \rfloor^{b_n} + [-L_d, L_d],
\end{cases} \tag{6}$$

where $a_i \in (0, 1)$, $b_i > 1, (i = \overline{1, n})$, and $L_d > 0$ are constants. Also, if the nonnegative constants $\rho_i, \bar{\rho}_i, (i = \overline{1, n})$ are assigned

to ensure the following A_1, A_2 matrices are Hurwitz, i.e., every eigenvalue of the matrices has a strictly negative real part:

$$A_1 = \begin{bmatrix} -\rho_1 & 1 & 0 \\ -\rho_2 & 0 & 1 \\ -\rho_3 & 0 & 0 \end{bmatrix}, A_2 = \begin{bmatrix} -\bar{\rho}_1 & 1 & 0 \\ -\bar{\rho}_2 & 0 & 1 \\ -\bar{\rho}_3 & 0 & 0 \end{bmatrix}. \tag{7}$$

Then, the system (6) is fixed-time stable, i.e., uniform settling-time w.r.t. initial condition.

Lemma 6 (see [52]). *Consider system (1). If there exist $\mathscr{C}^1$ Lyapunov function $V(x)$: $\mathbb{D} \to \mathbb{R}_+$ and some real constants $0 < c < \infty$ and $0 < \alpha < 1$, such that*

$$\dot{V}(x) \le -cV(x)^{\alpha}, \tag{8}$$

then, system (1) is finite-time stable for any given $x(t_0) \in D_0 \subseteq D$, in which the finite settling time T^* satisfies

$$T^* \le \frac{V(x)^{1-\alpha}}{c(1-\alpha)}. \tag{9}$$

2.2. Problem Formulation. The motion of the quadrotor in space can be described by a B-frame and an E-frame (see Figure 1). The vehicle moves and changes its attitude by virtue of an appropriate set of angular speeds of the rotors. The rotors generate the lift force denoted by $f_i \in \mathbb{R}_+$, $(i = \overline{1,4})$.

The E-frame is used to define the translational motion by $P \coloneqq [x, y, z]^T \in \mathbb{R}^3$. The B-frame indicates the rotational motion, i.e., Euler angles $\eta \coloneqq [\Phi, \theta, \psi]^T \in \mathbb{R}^3$. The 6-DoF acceleration dynamics corresponding to the rotation and translation motions of the quadrotor in the presence of disturbances can be written as [48]

$$\begin{cases} \ddot{\Phi} = J_{xx}^{-1}\left((J_{yy} - J_{zz})\dot{\theta}\dot{\psi} - c_{\Phi}\dot{\Phi}^2 - J_r\bar{\omega}\dot{\theta} + u_{\Phi} + d_{\Phi}^{\text{ext}} \right), \\ \ddot{\theta} = J_{yy}^{-1}\left((J_{zz} - J_{xx})\dot{\Phi}\dot{\psi} - c_{\theta}\dot{\theta}^2 + J_r\bar{\omega}\dot{\Phi} + u_{\theta} + d_{\theta}^{\text{ext}} \right), \\ \ddot{\psi} = J_{zz}^{-1}\left((J_{xx} - J_{yy})\dot{\Phi}\dot{\theta} - c_{\psi}\dot{\psi}^2 + u_{\psi} + d_{\psi}^{\text{ext}} \right), \end{cases} \tag{10}$$

$$\begin{cases} \ddot{x} = -m^{-1}\left((\mathrm{c}\Phi\mathrm{s}\theta\mathrm{c}\psi + \mathrm{s}\Phi\mathrm{s}\psi)u_z - k_x\dot{x} + d_x^{\text{ext}} \right), \\ \ddot{y} = -m^{-1}\left((\mathrm{c}\Phi\mathrm{s}\theta\mathrm{s}\psi - \mathrm{s}\Phi\mathrm{c}\psi)u_z - k_y\dot{y} + d_y^{\text{ext}} \right), \\ \ddot{z} = -m^{-1}\left((\mathrm{c}\Phi\mathrm{c}\theta)u_z - k_z\dot{z} + d_z^{\text{ext}} \right) + \mathrm{g}. \end{cases} \tag{11}$$

Since the flight of the quadcopter is driven by four propellers, the angular speeds of the four propellers Ω_i, $(i = \overline{1,4})$ determine the total lift force (thrust control input) u_z and the torques u_η. The quadrotor's actuators (rotors) produce a total lift force defined as [53]

$$u_z \coloneqq \sum_{j=1}^{4} f_i = c_t \sum_{j=1}^{4} \Omega_i^2. \tag{12}$$

The control torques u_η developed by the quadrotor's actuators are defined as [54]

$$u_\eta \coloneqq \begin{bmatrix} u_{\Phi} \\ u_{\theta} \\ u_{\psi} \end{bmatrix} = \begin{bmatrix} l(-f_1 + f_2 + f_3 - f_4) \\ l(f_1 - f_2 + f_3 - f_4) \\ c_d\left(-\Omega_1^2 - \Omega_2^2 + \Omega_3^2 + \Omega_4^2\right) \end{bmatrix}. \tag{13}$$

Besides, the rotating velocities of the four propellers, i.e., $\Omega_i, i = \overline{1,4}$, are related to u_η (the torques) and u_z (the total lift force) by the means of a constant invertible matrix as [55]

$$\begin{bmatrix} u_z \\ u_\eta \end{bmatrix} \coloneqq \begin{bmatrix} u_z \\ u_{\Phi} \\ u_{\theta} \\ u_{\psi} \end{bmatrix} = \begin{bmatrix} c_t & c_t & c_t & c_t \\ -lc_t & lc_t & lc_t & -lc_t \\ lc_t & -lc_t & lc_t & -lc_t \\ -c_d & -c_d & c_d & c_d \end{bmatrix} \begin{bmatrix} \Omega_1^2 \\ \Omega_2^2 \\ \Omega_3^2 \\ \Omega_4^2 \end{bmatrix}. \tag{14}$$

Remark 7. In practice, it is difficult to identify and to estimate the exact parameters of the quadrotor system, notably, the aerodynamic coefficients. Besides, model uncertainties are inevitably present in the dynamic model of the quadrotor. Therefore, in contrast to several reported works, e.g., [21, 37, 38] that consider a perfect model with precise knowledge of the model parameters, both model uncertainties and external time-varying disturbances are considered in the present study. Hence, the following assumption is introduced for the quadrotor dynamics given in (10) and (11).

Assumption 8. We assume in our study that the model uncertainties, i.e., internal unmodeled dynamics, are the aerodynamic and gyroscopic effect moments denoted by τ_a and τ_g, i.e.,

$$d_\eta^{\text{unc}} \coloneqq \begin{bmatrix} d_{\Phi}^{\text{unc}} \\ d_{\theta}^{\text{unc}} \\ d_{\psi}^{\text{unc}} \end{bmatrix} = \tau_a + \tau_g = \begin{bmatrix} -c_{\Phi}\dot{\Phi}^2 - J_r\bar{\omega}\dot{\theta} \\ -c_{\theta}\dot{\theta}^2 + J_r\bar{\omega}\dot{\Phi} \\ -c_{\psi}\dot{\psi}^2 \end{bmatrix}. \tag{15}$$

Since it is difficult to identify the aerodynamic coefficients $K_a = \mathrm{diag}\,(k_x, k_y, k_z)$ in practice, the unmodeled dynamics, for the translational subsystem, are the drag force F_a. These disturbances are defined as

$$d_P^{\text{unc}} \coloneqq \begin{bmatrix} d_x^{\text{unc}} \\ d_y^{\text{unc}} \\ d_z^{\text{unc}} \end{bmatrix} = F_a = \begin{bmatrix} -k_x v_x/m \\ -k_y v_y/m \\ -k_z v_z/m \end{bmatrix}. \tag{16}$$

Thus, the unmodeled dynamics for the quadrotor system are viewed as disturbances by the control law.

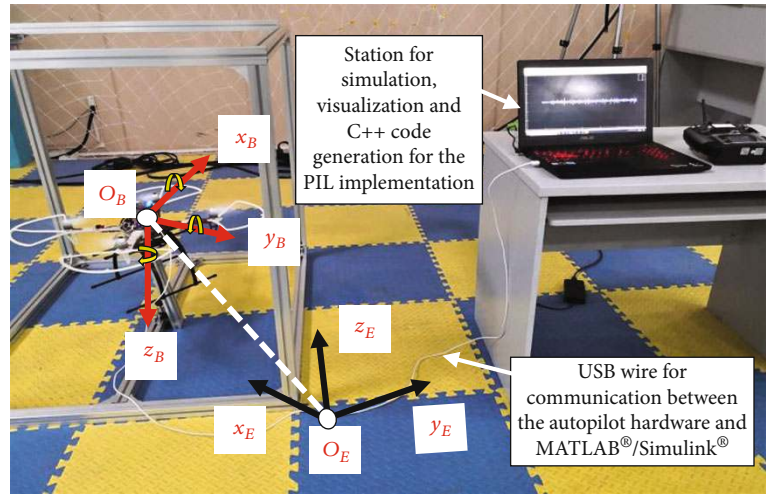

Figure 1: PIL experiment setup: quadrotor model with x-configuration represented in E-frame and B-frame.

Remark 9. Since the internal unmodeled dynamics and uncertainties are considered as a part of the total disturbances, Assumption 8 will not affect the system stability and control performance. Therefore, the model uncertainties $d_\eta^{\text{unc}}, d_P^{\text{unc}}$ can be dealt with by the FTO and the FXESO, respectively. Thus, the simplifications of the mathematical model adopted in Assumption 8 are reasonable and can be accepted within the proposed TSMBAADC strategy.

Finally, by choosing $\chi \coloneqq [x, \dot{x}, y, \dot{y}, z, \dot{z}, \Phi, \dot{\Phi}, \theta, \dot{\theta}, \psi, \dot{\psi}] \in \mathbb{R}^{12}$ as a state vector, the following state-space model for the 6-DoF quadrotor dynamics is obtained:

$$\begin{cases} \dot{\chi}_1 = \chi_2, \\ \dot{\chi}_2 = -m^{-1}[(c\chi_7 cs\chi_9 + s\chi_7 s\psi)u_z + d_x], \\ \dot{\chi}_3 = \chi_4, \\ \dot{\chi}_4 = -m^{-1}\left[(c\chi_7 s\chi_{11} s\chi_9 - c\chi_{11} s\chi_7)u_z + d_y\right], \\ \dot{\chi}_5 = \chi_6, \\ \dot{\chi}_6 = -m^{-1}[(c\chi_7 c\chi_9)u_z + d_z] + \mathrm{g}, \\ \dot{\chi}_7 = \chi_8, \\ \dot{\chi}_8 = J_{xx}^{-1}\left[\left(J_{yy} - J_{zz}\right)\chi_{10}\chi_{12} + u_\Phi + d_\Phi\right], \\ \dot{\chi}_9 = \chi_{10}, \\ \dot{\chi}_{10} = J_{yy}^{-1}[(J_{zz} - J_{xx})\chi_8\chi_{12} + u_\theta + d_\theta], \\ \dot{\chi}_{11} = \chi_{12}, \\ \dot{\chi}_{12} = J_{zz}^{-1}\left[\left(J_{xx} - J_{yy}\right)\chi_8\chi_{10} + u_\psi + d_\psi\right]. \end{cases} \tag{17}$$

The control problem of our study is formulated mathematically in the following definition.

Definition 10. (Robust finite-time trajectory tracking control problem).

The considered control problem of our study consists of designing robust finite-time TSM control laws $u_\eta(t) = [u_\Phi, u_\theta, u_\psi]^T$ and $u_z(t)$ for both attitude and position subsystems affected by perturbations in (17), such that

(i) The attitude and position tracking errors tend to the origin in a fast finite-time, i.e., for $\forall e_\eta(t) \coloneqq \eta(t) - \eta_d(t), \forall e_P(t) \coloneqq P(t) - P_d(t)$, there exist two constants T_1, T_3, such that

$$\begin{cases} \lim\limits_{t \to T_1} e_\eta(t) = 0, \forall t > T_1, \\ \lim\limits_{t \to T_3} e_P(t) = 0, \forall t > T_3, \end{cases} \tag{18}$$

where $\eta_d(t)$ and $P_d(t)$ are the desired reference signals for the attitude and position subsystems, respectively.

(i) The controller must ensure good robustness against lumped disturbances (model uncertainties, parameter variation, and external time-varying wind disturbances)

(ii) The control signal is nonsingular, continuous, and chattering-free

3. Flight Control System Design

The control system design is aimed at realizing a robust Cartesian trajectory tracking for the quadrotor system subjected to lumped disturbances. This can be attained through a robust tracking of the position and attitude references.

The quadrotor system (17) is a nonlinear system with underactuated dynamics. This system has six output variables $(x, y, z, \Phi, \theta, \psi)$ but only four control inputs are available $(u_z, u_\Phi, u_\theta, u_\psi)$. Notably, the translational movements of the vehicle are directly achieved by the rotational

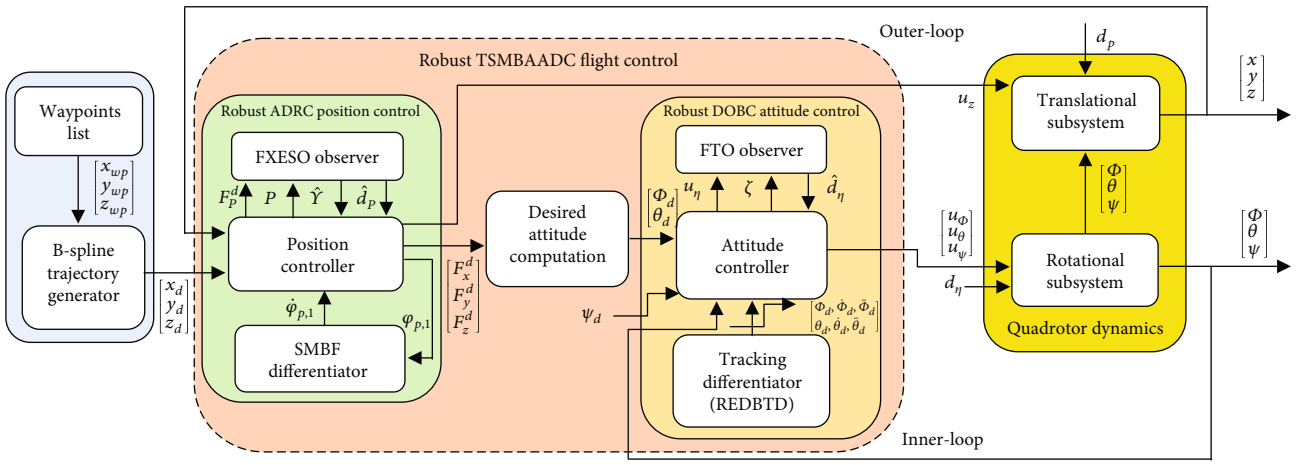

FIGURE 2: Block diagram of the quadrotor aircraft depicting the proposed flight control structure.

motions. To deal with this problem, the hierarchical control structure is adopted as depicted in Figure 2. In the context of the hierarchical control scheme, the flight control of the quadrotor system is divided into two control loops: an inner loop for the rotational subsystem and an outer loop for the translational subsystem. The inner loop corresponds to the CNTSMC that ensures attitude stability of the quadrotor by controlling the angular variables. The input of this control loop is the reference angles $(\Phi_d, \theta_d, \psi_d)$, and the output is the appropriate roll, pitch, and yaw torques $(u_\Phi, u_\theta, u_\psi)$. A BSITSMC is synthesized for the outer loop to achieve robust position tracking. This loop takes the desired position signals (x_d, y_d, z_d) as input and generates the reference angles (Φ_d, θ_d) for the inner loop and also the total thrust force control u_z.

3.1. Attitude Control Design. In this subsection, a tracking differentiator (TD) is introduced to estimate the desired attitude target signals and their first and second derivatives. Subsequently, the DOBC structure is designed for the rotational subsystem so that the target signals are tracked in finite time.

3.1.1. Tracking Differentiator. In practice, it is more reliable to use the technique of differentiators in the implementation process of the control algorithm. Thus, a TD is designed to supply the estimates of (Φ_d, θ_d), $(\dot{\Phi}_d, \dot{\theta}_d)$, and $(\ddot{\Phi}_d, \ddot{\theta}_d)$ for the controller. To this end, a robust exact differentiator-based TD (REDBTD) is adopted [56], which is defined as

$$\begin{cases} \dot{\widehat{\varkappa}}_{d,0} = k_0 \left[\varkappa_d - \varkappa\wedge_{d,0}\right]^{2/3} + \widehat{\varkappa}_{d,1}, \\ \dot{\widehat{\varkappa}}_{d,1} = k_1 \left[\varkappa_d - \varkappa\wedge_{d,0}\right]^{1/3} + \widehat{\varkappa}_{d,2}, \\ \dot{\widehat{\varkappa}}_{d,2} = k_2 \ \text{sign}\ (\varkappa_d - \widehat{\varkappa}_{d,0}), \end{cases} \tag{19}$$

where $\varkappa_d$ is the signal to be differentiated and $\varkappa_d = \{\Phi_d, \theta_d\}$. Then, $\widehat{\varkappa}_{d,0}$, $\widehat{\varkappa}_{d,1}$ and $\widehat{\varkappa}_{d,2}$ are the finite-time estimates of $\varkappa_d, \dot{\varkappa}_d$ and $\ddot{\varkappa}_d$, respectively, i.e., $\widehat{\varkappa}_{d,0} \to \varkappa_d, \widehat{\varkappa}_{d,1} \to \dot{\varkappa}_d$, and $\widehat{\varkappa}_{d,2} \to \ddot{\varkappa}_d$.

3.1.2. Disturbance Observer Design for the Attitude Loop. A convenient model is established to facilitate the design of the controller and disturbance observer. Therefore, from the quadrotor model given in (17), the following attitude dynamic model can be established:

$$\begin{cases} \dot{X}_1(t) = X_2(t), \\ \dot{X}_2(t) = f_\eta(X_2, t) + g_\eta(t)\left(u_\eta(t) + d_\eta(t)\right), \\ \mathcal{Y}_1(t) = X_1(t). \end{cases} \tag{20}$$

Here, $X_\eta \coloneqq [X_1, X_2]^T \in \mathbb{R}^{3\times 2}$ is the states vector, where $X_1 \coloneqq \eta = [\chi_7, \chi_9, \chi_{11}]^T = [\Phi, \theta, \psi]^T \in \mathbb{R}^3, X_2 \coloneqq \dot{\eta} = [\dot{\Phi}, \dot{\theta}, \dot{\psi}]^T = [\chi_8, \chi_{10}, \chi_{12}]^T \in \mathbb{R}^3$, $u_\eta \coloneqq [u_\Phi, u_\theta, u_\psi]^T \in \mathbb{R}^3$ is the control inputs vector, $\mathcal{Y}_1 \coloneqq [\Phi, \theta, \psi]^T \in \mathbb{R}^3$is the controlled outputs vector, and the uncertain function $d_\eta \coloneqq d_\eta^{\text{unc}} + d_\eta^{\text{ext}}$ stands for the total disturbances. The external disturbances are modeled as sinusoidal signals with different frequencies. Thus, they are considered Lipschitz continuous matched disturbances with bounded derivatives [57]. Hence, the unknown disturbances d_η behave as a sufficiently smooth uncertain function with its first-time derivative satisfying $\|\dot{d}_\eta\| \le l_\eta$, where l_η is a nonnegative bounded constant, i.e., $0 < l_\eta < \infty$ [51, 58]. The functions $f_\eta(X_2, t), g_\eta(t)$ are defined as

$$f_\eta \coloneqq \begin{bmatrix} f_\Phi \\ f_\theta \\ f_\psi \end{bmatrix} = \begin{bmatrix} J_{xx}^{-1}(J_{yy} - J_{zz})\chi_{10}\chi_{12} \\ J_{yy}^{-1}(J_{zz} - J_{xx})\chi_8\chi_{12} \\ J_{zz}^{-1}(J_{xx} - J_{yy})\chi_8\chi_{10} \end{bmatrix},$$

$$g_\eta \coloneqq \left[g_\Phi g_\theta g_\psi\right]^T = \left[J_{xx}^{-1} J_{yy}^{-1} J_{zz}^{-1}\right]^T. \tag{21}$$

The model that we have established in (20) is a general description of the attitude system with nonlinear second-order dynamics associated with roll, pitch, and yaw motions in the presence of disturbances.

Theorem 11. *Given the attitude dynamic model described in the presence of disturbances (20), an FTO observer is designed as*

$$\begin{cases} \dot{\Gamma}_0^\eta = ?_0 + f_\eta + g_\eta u_\eta, \\ ?_0 = -\rho_1^\eta l_\eta^{1/3} \left|\Gamma_0^\eta - \dot{\eta}\right|^{2/3} \operatorname{sign}\left(\Gamma_0^\eta - \dot{\eta}\right) + \Gamma_1^\eta, \\ \dot{\Gamma}_1^\eta = ?_1, \\ ?_1 = -\rho_2^\eta l_\eta^{1/2} \left|\Gamma_1^\eta - ?_0\right|^{1/2} \operatorname{sign}\left(\Gamma_1^\eta - ?_0\right) + \Gamma_2^\eta, \\ \dot{\Gamma}_2^\eta = -\rho_3^\eta l_\eta \operatorname{sign}\left(\Gamma_2^\eta - ?_1\right), \end{cases} \tag{22}$$

where Γ_2^η is the estimate of d_η. Then, the disturbance d_η can be precisely identified within a finite-time T_0, i.e., $d_\eta \equiv \widehat{d}_\eta$.

Proof. Let us define the observation errors as

$$\begin{cases} \ell_1^\eta \coloneqq \Gamma_0^\eta - \dot{\eta}, \\ \ell_2^\eta \coloneqq \Gamma_1^\eta - d_\eta, \\ \ell_3^\eta \coloneqq \Gamma_2^\eta - \dot{d}_\eta. \end{cases} \tag{23}$$

By differentiating these errors w.r.t time and substituting $\ddot{\eta}, \dot{\Gamma}_0^\eta, \dot{\Gamma}_1^\eta, \dot{\Gamma}_2^\eta$ by their expressions, the corresponding error dynamics can be written as

$$\begin{cases} \dot{\ell}_1^\eta = -\rho_1^\eta l_\eta^{1/3} \left|\Gamma_0^\eta - \dot{\eta}\right|^{2/3} \operatorname{sign}\left(\Gamma_0^\eta - \dot{\eta}\right) + \Gamma_1^\eta - d_\eta, \\ \dot{\ell}_2^\eta = -\rho_2^\eta l_\eta^{1/2} \left|\Gamma_1^\eta - ?_0\right|^{1/2} \operatorname{sign}\left(\Gamma_1^\eta - ?_0\right) + \Gamma_2^\eta - \dot{d}_\eta \\ \dot{\ell}_3^\eta = -\rho_3^\eta l_\eta \operatorname{sign}\left(\Gamma_2^\eta - ?_1\right) - \ddot{d}_\eta. \end{cases} \tag{24}$$

Then, by substituting Λ_0, Λ_1 by their expressions, and after some manipulations, we get

$$\begin{cases} \dot{\ell}_1^\eta = -\rho_1^\eta l_\eta^{1/3} \left|\ell_1^\eta\right|^{2/3} \operatorname{sign}\left(\ell_1^\eta\right) + \ell_2^\eta, \\ \dot{\ell}_2^\eta = -\rho_2^\eta l_\eta^{1/2} \left|\ell_2^\eta - \dot{\ell}_1^\eta\right|^{1/2} \operatorname{sign}\left(\ell_2^\eta - \dot{\ell}_1^\eta\right) + \ell_3^\eta, \\ \dot{\ell}_3^\eta = -\rho_3^\eta l_\eta \operatorname{sign}\left(\ell_3^\eta - \dot{\ell}_2^\eta\right) - \ddot{d}_\eta. \end{cases} \tag{25}$$

Based on Lemma 2, the observation errors $(\ell_1^\eta, \ell_2^\eta, \ell_3^\eta)$ are finite-time convergent to the origin within the time T_0, i.e., $\Gamma_1^\eta \equiv \widehat{d}_\eta$.

3.1.3. Finite-Time Continuous Nonsingular Terminal Sliding Mode Control Design. Let $X_{1d} \coloneqq \eta_d = [\chi_7^d, \chi_9^d, \chi_{11}^d]^T = [\Phi_d, \theta_d, \psi_d]^T \in \mathbb{R}^3$ be the reference attitude and X_1 be the actual attitude. Let us define the attitude tracking errors as

$$\begin{cases} e_\eta \coloneqq X_1 - X_{1d}, \\ \varrho_\eta \coloneqq \dot{X}_1 - \dot{X}_{1d}, \end{cases} \tag{26}$$

where $e_\eta \coloneqq [e_{\chi_7}, e_{\chi_9}, e_{\chi_{11}}]^T, \varrho_\eta \coloneqq \dot{e}_\eta = [\varrho_{\chi_7}, \varrho_{\chi_9}, \varrho_{\chi_{11}}]^T$. The tracking errors dynamics is given as

$$\begin{cases} \dot{e}_\eta = \varrho_\eta, \\ \dot{\varrho}_\eta = \ddot{X}_1 - \ddot{X}_{1d}. \end{cases} \tag{27}$$

The control objective for the attitude system is to make the X_1 states track the desired reference X_{1d} by designing a continuous-SMC law $u_\eta = [u_\Phi, u_\theta, u_\psi]^T$. Then, the tracking errors vector can be stabilized to zero, i.e., $e_\eta \equiv 0$. Let $e_1^\eta \coloneqq e_\eta$ and $e_2^\eta \coloneqq \dot{e}_\eta$. To ensure fast convergence of attitude variables to their reference signals, the following CNTSM surface is proposed for the rotational system (19)

$$s_\eta \coloneqq \dot{e}_2^\eta + \sum_{j=1}^{n} k_j^\eta \left(\left\lceil e_j^\eta \right\rfloor^{\alpha_{1,j}} + \left\lceil e_j^\eta \right\rfloor + \left\lceil e_j^\eta \right\rfloor^{\alpha_{2,j}} \right), \tag{28}$$

where the nonnegative parameters $k_j^\eta, \alpha_{1,j}$, and $\alpha_{2,j}$ are chosen based on Remark 13 which is drawn hereafter. The control action is applied to establish the reaching phase of the sliding surface s_η, and the sliding motion on $s_\eta = 0$ is determined as follows [59]:

$$u_\eta \coloneqq u_{eq_\eta} + g_\eta^{-1} u_{r_\eta}. \tag{29}$$

This control structure consists of two parts; the term u_{eq_η} is the equivalent control part, which maintains the variables on the sliding surface, and u_{r_η} is the reaching control part, which ensures faster convergence. On the one hand, the u_{eq_η} control can be obtained from the sliding motion $s_\eta = 0$. Thus, when $s_\eta = 0$, we get

$$\dot{e}_2^\eta + \sum_{j=1}^{n} k_j^\eta \left(\left\lceil e_j^\eta \right\rfloor^{\alpha_{1,j}} + \left\lceil e_j^\eta \right\rfloor + \left\lceil e_j^\eta \right\rfloor^{\alpha_{2,j}} \right) = 0, \tag{30}$$

where $\dot{e}_\eta \coloneqq \ddot{X}_1 - \ddot{X}_{1d}$. Substituting $\ddot{X}_1$ by its expression from (20) into (30), and after some manipulations, the equivalent control can be obtained as

$$u_{eq_\eta} = g_\eta^{-1}\left[-f_\eta - \ddot{e}_2^\eta + \sum_{j=1}^{n} k_j^\eta \left(\left\lceil e_j^\eta \right\rfloor^{\alpha_{1,j}} + \left\lceil e_j^\eta \right\rfloor^{\alpha_{2,j}}\right) - \widehat{d}_\eta + \ddot{\eta}_d\right], \tag{31}$$

where $\ddot{\eta}_d = \ddot{X}_{1d}$, $\widehat{d}_\eta$ is estimated by the FTO observer given by (22). On the other hand, the u_{r_η} control is chosen to ensure the finite-time reaching of the sliding surface, and it is proposed as

$$\dot{u}_{n_\eta} := -\lambda_\eta \left\lceil s_\eta \right\rfloor^{\xi} - \mu_\eta \left\lceil s_\eta \right\rfloor^{\varepsilon}. \tag{32}$$

Therefore, using (31) and (32), the final attitude control is given as

$$u_\eta = g_\eta^{-1}\left[-f_\eta - \ddot{e}_2^\eta + \sum_{j=1}^{n} k_j^\eta \left(\left\lceil e_j^\eta \right\rfloor^{\alpha_{1,j}} + \left\lceil e_j^\eta \right\rfloor^{\alpha_{2,j}}\right) - \widehat{d}_\eta + \ddot{\eta}_d + u_{n_\eta}\right]. \tag{33}$$

Finally, by replacing η with (Φ, θ, ψ), the corresponding roll, pitch, and yaw control laws can be deduced.

Remark 12. In contrast to many reported control laws suffering from the singularity problem, our control law is designed to be singularity-free. It is worth mentioning that since the derivatives of the terms $\lceil e_j^\eta \rfloor^{\alpha_{1,j}}$, $\lceil s_\eta \rfloor^{\varepsilon}$ with fractional power $(\alpha_{1,j}, \varepsilon < 1)$ are not required in the expression of the control law (33), it results that the singularity problem is avoided, i.e., the magnitude of the control signal does not tend to the infinity. The singularity problem may occur when there exists a term with a negative power in the control signal. For example, the singularity will happen if the derivative of $\lceil e_j^\eta \rfloor^{\alpha_{1,j}}$ exists in the control, that is, $\lim_{e_j^\eta \to 0} d\lceil e_j^\eta \rfloor^{\alpha_{1,j}}/dt := \lim_{e_j^\eta \to 0} \alpha_{1,j} |e_j^\eta|^{\alpha_{1,j}-1} \dot{e}_{i,j}^\eta = \infty$, since $\alpha_{1,j} - 1 < 0$.

Remark 13. In this study, rigorous conditions are established for the choice of the control parameters. On one hand, the exponents $\alpha_{1,j}, \alpha_{2,j}, (j = \overline{1,2})$ are chosen based on homogeneity theory as follows [50]: $\alpha_{1,n-k} = \bar{\alpha}/(k(1-\bar{\alpha})+1)$ and $\alpha_{2,n-k} = (2-\bar{\alpha})/(k(\bar{\alpha}-1)+1)$, where $\bar{\alpha} \in (\epsilon, 1)$, $\epsilon \in (n-2/n-1, 1)$ and $k = \overline{0, n-1}$. To ensure the finite-time convergence feature, $\alpha_{1,j}, \alpha_{2,j}, (j = \overline{1,2})$ should satisfy $\alpha_{1,1}, \alpha_{1,2} < 1$, and $\alpha_{2,1}, \alpha_{2,2} > 1$. On the other hand, the positive constants $k_j^\eta > 0, (j = \overline{1,n})$ should be selected to make the n-order polynomials $s^n + k_n s^{n-1} + \cdots + k_2 s + k_1$ and $s^n + 3k_n s^{n-1} + \cdots + 3k_2 s + 3k_1$ be Hurwitz in terms of the Laplace operator s. Besides, the positive constants $\lambda_\eta, \mu_\eta > 0$, $\xi > 1$ and $\varepsilon < 1$ are chosen to preadjust a settling-time for the reaching phase of the sliding mode as it is shown in Lemma 4. In addition, the positive parameters of the observer $\rho_i^\eta > 0, (i = \overline{1,3})$ should be selected to satisfy the following condition $\rho_1^\eta > \rho_2^\eta > \rho_3^\eta$. The parameter l_η is the upper bound of the total disturbances. It is a bounded constant $0 < l_\eta < \infty$.

3.1.4. Stability Analysis for the Attitude Closed-Loop System

Theorem 14. *For the nonlinear perturbated attitude system given by (20), if the control law u_η is designed by (33), and employing disturbance observer (22), then, the attitude system is finite-time stable within a bounded time T_1, i.e., $e_\eta(t) \equiv 0$, $\forall t \geq T_1$.*

Proof. The proof of the theorem is based on two consecutive steps. First, we prove that the sliding manifold is reached in finite time. Second, we show that the tracking errors of the attitude system tend to zero along with the sliding manifold in finite-time.

Step 1: By substituting $\ddot{\eta}$ from (20) into the sliding surface s_η (28), we get

$$s_\eta = f_\eta + g_\eta\left(u_\eta + d_\eta\right) - \ddot{\eta}_d + \sum_{j=1}^{n} k_j^\eta \left(\left\lceil e_j^\eta \right\rfloor^{\alpha_{1,j}} + \left\lceil e_j^\eta \right\rfloor + \left\lceil e_j^\eta \right\rfloor^{\alpha_{2,j}}\right). \tag{34}$$

Then, by substituting the designed control law u_η (33) into s_η given in (34), the sliding surface dynamics becomes as

$$s_\eta = u_{r_\eta} + d_\eta - \widehat{d}_\eta. \tag{35}$$

By Theorem 11, we have $d_\eta \equiv \widehat{d}_\eta$ for all $t \geq T_0$. Hence, we get

$$s_\eta = u_{r_\eta}. \tag{36}$$

By differentiating (36) and substituting (32), it yields

$$\dot{s}_\eta = \dot{u}_{r_\eta} = -\lambda_\eta \left\lceil s_\eta \right\rfloor^{\xi} - \mu_\eta \left\lceil s_\eta \right\rfloor^{\varepsilon}. \tag{37}$$

Subsequently, let us define the following positive-definite Lyapunov function:

$$V_\eta\left(s_\eta\right) := \frac{s_\eta^2}{2}, \tag{38}$$

By differentiating V_η and substituting (37), it yields

$$\dot{V}_\eta\left(s_\eta\right) = s_\eta \dot{s}_\eta = s_\eta\left(-\lambda_\eta \left\lceil s_\eta \right\rfloor^{\xi} - \mu_\eta \left\lceil s_\eta \right\rfloor^{\varepsilon}\right), = -\lambda_\eta s_\eta \left\lceil s_\eta \right\rfloor^{\xi} - \mu_\eta s_\eta \left\lceil s_\eta \right\rfloor^{\varepsilon}. \tag{39}$$

By using $s_\eta = \lceil s_\eta \rfloor$ and $\lceil s_\eta \rfloor \lceil s_\eta \rfloor^{\xi} = |s_\eta||s_\eta|^{\xi}$, we get

$$\dot{V}_\eta\left(s_\eta\right) \leq -\lambda_\eta \left|s_\eta\right|^{\xi+1} - \mu_\eta \left|s_\eta\right|^{\varepsilon+1}, \leq -\lambda_\eta V_\eta^{(\xi+1)/2} - \mu_\eta V_\eta^{(\varepsilon+1)/2}. \tag{40}$$

By considering that $\xi > 1, \varepsilon \in (0,1)$, it yields $(\xi+1)/2 > 1$ and $(\varepsilon+1)/2 < 1$. According to Lemma 4, the finite-time reaching of sliding surface $s_\eta = 0$ is guaranteed within the following bounded reaching-time $T_r \le T^\star := 1/\lambda_\eta(((\xi+1)/2) - 1) + 1/\mu_\eta(1 - ((\varepsilon+1)/2))$.

Step 2: Recalling the errors dynamics for the angular signals given in (27)

$$\begin{cases} \dot{e}_\eta = \varrho_\eta, \\ \dot{\varrho}_\eta = \ddot{\eta} - \ddot{\eta}_d. \end{cases} \tag{41}$$

We define $\bar{x}_1 := e_\eta = e_1^\eta$, $\bar{x}_2 := \dot{e}_\eta = \varrho_\eta = e_2^\eta$ and $\bar{x} := [\bar{x}_1, \bar{x}_2]^T$. Consequently, the closed-loop dynamics (41) can be rewritten as

$$\begin{cases} \dot{\bar{x}}_1 = \bar{x}_2, \\ \dot{\bar{x}}_2 = \ddot{\eta} - \ddot{\eta}_d. \end{cases} \tag{42}$$

When $s_\eta = 0$, from (28) and considering $\bar{x}_1 = e_\eta, \bar{x}_2 = \varrho_\eta$, we have

$$\ddot{\eta} = \ddot{\eta}_d - k_1^\eta(\lceil \bar{x}_1 \rfloor^{\alpha_{1,1}} + \lceil \bar{x}_1 \rfloor + \lceil \bar{x}_1 \rfloor^{\alpha_{2,1}}) - k_2^\eta(\lceil \bar{x}_2 \rfloor^{\alpha_{1,2}} + \lceil \bar{x}_2 \rfloor + \lceil \bar{x}_2 \rfloor^{\alpha_{2,2}}). \tag{43}$$

Substituting (43) into error dynamics expressions (42), we get

$$\begin{cases} \dot{\bar{x}}_1 = \bar{x}_2, \\ \dot{\bar{x}}_2 = -k_1^\eta(\lceil \bar{x}_1 \rfloor^{\alpha_{1,1}} + \lceil \bar{x}_1 \rfloor + \lceil \bar{x}_1 \rfloor^{\alpha_{2,1}}) - k_2^\eta(\lceil \bar{x}_2 \rfloor^{\alpha_{1,2}} + \lceil \bar{x}_2 \rfloor + \lceil \bar{x}_2 \rfloor^{\alpha_{2,2}}). \end{cases} \tag{44}$$

According to Lemma 3, we can deduce that the tracking error dynamics (44) can be stabilized to zero during the sliding motion $s_\eta = 0$ within a finite bounded time. Thus, there exists a constant T_s such that $e_\eta \to 0$ and $\varrho_\eta \to 0$ for all $t \ge T_1 := T_0 + T_r + T_s$. This completes the proof.

3.2. Position Control Design. The synthesis of the position controller is divided into two steps. In the first step, the disturbance observer is addressed; while in the second step, the robust backstepping sliding mode controller is developed.

3.2.1. FXESO Observer Design for the Position Loop. The quadrotor translational system is divided into three second-order subsystems, the altitude z, and the horizontal position x, y. Thus, the following translational system subjected to disturbances can be obtained from (17) as

$$\begin{cases} \dot{X}_3(t) = X_4(t), \\ \dot{X}_4(t) = f_P(X_4, t) + F_P(X_1, t) + d_P(t), \\ \mathcal{Y}_2(t) = X_4(t). \end{cases} \tag{45}$$

Here, $X_P := [X_3, X_4]^T \in \mathbb{R}^{3\times 2}$ is the states vector, where $X_3 := P = [\chi_1, \chi_3, \chi_5]^T = [x, y, z]^T \in \mathbb{R}^3$, $X_4 := \dot{P} = Y = [\dot{x}, \dot{y}, \dot{z}]^T = [\chi_2, \chi_6, \chi_8]^T \in \mathbb{R}^3$, $\mathcal{Y}_2 := [x, y, z]^T$ is the controlled outputs vector, and the uncertain function $d_P(t) := d_P^{\text{unc}} + d_P^{\text{ext}}$ summarizes the total lumped disturbances including model uncertainty effects, parameters' uncertainties, and external disturbances, where $\|\dot{d}_P(t)\| \le l_P$ and $0 < l_P < \infty$. The functions $f_P(X_4, t)$, $F_P(X_1, t)$ are defined as

$$f_P(X_4, t) := F_a = K_a X_4, \tag{46}$$

$$F_P := \begin{bmatrix} F_x \\ F_y \\ F_z \end{bmatrix} = \begin{bmatrix} -u_z m^{-1}\left(\mathrm{c}\chi_7^d \mathrm{c}\chi_{11}^d \mathrm{s}\chi_9^d + \mathrm{s}\chi_7^d \mathrm{s}\chi_{11}^d\right) \\ -u_z m^{-1}\left(\mathrm{c}\chi_7^d \mathrm{s}\chi_{11}^d \mathrm{s}\chi_9^d - \mathrm{c}\chi_{11}^d \mathrm{s}\chi_7^d\right) \\ -u_z m^{-1}\left(\mathrm{c}\chi_{11}^d \mathrm{c}\chi_9^d\right) + \mathrm{g} \end{bmatrix}. \tag{47}$$

Given the disturbed position dynamic model described in (45), the FXESO observer is designed as

$$\begin{cases} \dot{\Gamma}_1^P = \Gamma_2^P + \rho_1^P \lceil \ell_1^P \rfloor^{a_1} + \bar{\rho}_1^P \lceil \ell_1^P \rfloor^{b_1}, \\ \dot{\Gamma}_2^P = \Gamma_3^P + \mathcal{F}_P + \rho_2^P \lceil \ell_1^P \rfloor^{a_2} + \bar{\rho}_2^P \lceil \ell_1^P \rfloor^{b_2}, \\ \dot{\Gamma}_3^P = \rho_3^P \lceil \ell_1^P \rfloor^{a_3} + \bar{\rho}_3^P \lceil \ell_1^P \rfloor^{b_3} + l_P \operatorname{sign}(\ell_1^P). \end{cases} \tag{48}$$

Then, the disturbances and the velocities can be estimated within a fixed bounded time T_2 as in (52); hereafter, i.e., $\Gamma_3^P := \widehat{d}_P \equiv d_P$ and $\Gamma_2^P := \widehat{Y} \equiv Y$. The exponents a_i, b_i are selected as follows: $a_i \in (0,1), i = \overline{1,3}$ satisfy the recurrent relations $a_i = i\bar{a} - (i-1), i = \overline{2,3}$, and $a_1 = \bar{a}$ where $\bar{a} \in (1 - \varepsilon_1, 1)$ for a sufficiently small $\varepsilon_1 > 0$. Also, $b_i > 1, i = \overline{1,3}$, and $b_i = i\bar{b} - (i-1), i = \overline{2,3}$, and $b = \bar{b}$ where $\bar{b} \in (1, 1+\varepsilon_2)$ for a sufficiently small $\varepsilon_2 > 0$. Besides, $\ell_1^P := P - \widehat{P}$ is the observation error and $\mathcal{F}_P := f_P + F_P$.

In (48), the terms $\lceil \ell_1^P \rfloor^{a_i}$ and $\lceil \ell_1^P \rfloor^{b_i}$ are continuous and differentiable. However, the term sign (ℓ_1^P) is discontinuous. Thus, to avoid the chattering effect and to realize the observer in practice, the following sigmoid function is used:

$$\operatorname{sgmf}(\ell_1^P) := \begin{cases} \left(\dfrac{2}{1 + \exp\left(-h\ell_1^P\right)}\right) - 1, & \left|\ell_1^P\right| \le \delta, \\ \operatorname{sign}(\ell_1^P), & \left|\ell_1^P\right| > \delta, \end{cases} \tag{49}$$

where h is a constant that is inversely proportional to δ, i.e., $\delta = 1/h$.

Theorem 15. *The FXESO observer designed in (48) can precisely estimate the disturbance and the velocities within a fixed bounded time T_2, i.e., $\Gamma_3^P := \widehat{d}_P \equiv d_P$ and $\Gamma_2^P := \widehat{Y} \equiv Y$.*

Proof. Let us define the observation errors as

$$\begin{cases} \ell_1^P \coloneqq P - \widehat{P}, \\ \ell_2^P \coloneqq Y - \widehat{Y}, \\ \ell_3^P \coloneqq d_P - \widehat{d}_P. \end{cases} \tag{50}$$

By differentiating these errors w.r.t time, it yields

$$\begin{cases} \dot{\ell}_1^P = \ell_2^P - \rho_1^P \lceil \ell_1^P \rfloor^{a_1} - \bar{\rho}_1^P \lceil \ell_1^P \rfloor^{b_1}, \\ \dot{\ell}_2^P = \ell_3^P - \rho_2^P \lceil \ell_1^P \rfloor^{a_2} - \bar{\rho}_2^P \lceil \ell_1^P \rfloor^{b_2}, \\ \dot{\ell}_3^P = \dot{d}_P - \rho_3^P \lceil \ell_1^P \rfloor^{a_3} - \bar{\rho}_3^P \lceil \ell_1^P \rfloor^{b_3} - l_P \mathrm{sgmf}(\ell_1^P). \end{cases} \tag{51}$$

Based on Lemma 5, the observation errors $(\ell_1^P, \ell_2^P, \ell_3^P)$ are guaranteed to converge to the origin in fixed-time bounded as

$$T_2 \leq \frac{\lambda_{\max}^{\Lambda}(P_1)}{\Xi_1 \Lambda} + \frac{1}{\Xi_2 \sigma \bar{\omega}^{\sigma}}, \tag{52}$$

where $\Xi_1 = \lambda_{\min}(Q_1)/\lambda_{\max}(P_1)$, $\Xi_2 = \lambda_{\min}(Q_2)/\lambda_{\max}(P_2)$, $\Lambda = 1 - \bar{a}$, $\sigma = \bar{b} - 1$, and $\bar{\omega} \leq \lambda_{\min}(P_2)$. Q_1, Q_2, P_1 and P_2 are nonsingular, symmetric, and positive-definite matrices and satisfy $P_1 A_1 + A_1^T = Q_1, P_2 A_2 + A_2^T = Q_2$.

3.2.2. Backstepping Integral Terminal Sliding Mode Control Design. The control law is designed for the position x here. Without loss of generality, the appropriate control laws for the y and z positions can be derived similarly.

Let x_d be the desired trajectory of the position x. The tracking error is defined as

$$e_x \coloneqq x - x_d. \tag{53}$$

To ensure fast finite-time convergence to the desired reference signal and to simultaneously ensure null steady-state error, the following integral terminal sliding surface is designed:

$$s_{x,1} \coloneqq k_{x,1} e_x + k_{x,2} \int |e_x|^{\alpha} \operatorname{sign}(e_x) dt. \tag{54}$$

Let us define the following Lyapunov function:

$$V_{e_x} \coloneqq \frac{e_x^2}{2}. \tag{55}$$

The time derivative of V_{e_x} is given as

$$\dot{V}_{e_x} = e_x \dot{e}_x. \tag{56}$$

In (56), the term $\dot{e}_x$ can be calculated from the sliding motion $\dot{s}_{x,1} = 0$ as

$$\dot{e}_x = -\frac{k_{x,2}}{k_{x,1}} |e_x|^{\alpha} \operatorname{sign}(e_x). \tag{57}$$

Therefore, $\dot{V}_{e_x}$ becomes

$$\begin{aligned} \dot{V}_{e_x} &= -\frac{k_{x,2}}{k_{x,1}} |e_x|^{\alpha} \operatorname{sign}(e_x) e_x \leq -\frac{k_{x,2}}{k_{x,1}} |e_x|^{(\alpha+1)}, \\ &\leq -\frac{k_{x,2}}{k_{x,1}} \left(e_x^2\right)^{\alpha+1/2} = -\frac{2^{\alpha+1/2} k_{x,2}}{k_{x,1}} \left(\frac{e_x^2}{2}\right)^{\alpha+1/2}, \\ &= -\frac{2^{\alpha+1/2} k_{x,2}}{k_{x,1}} \left(V_{e_x}\right)^{\alpha+1/2} \leq 0. \end{aligned} \tag{58}$$

Let us define ς and ϑ, respectively, as follows: $\varsigma \coloneqq 2^{\alpha+1/2} k_{x,2}/k_{x,1}$ and $\vartheta \coloneqq \alpha + 1/2$. Then, we can get

$$\dot{V}_{e_x} \leq -\varsigma V_{e_x}^{\vartheta}. \tag{59}$$

It follows from Lemma 6 that the convergence of the tracking errors for the position x can be achieved within a finite-time T_3, bounded as

$$T_3 \leq \frac{V_{e_{x,0}}^{1-\vartheta}}{\varsigma(1-\vartheta)}, \tag{60}$$

where $V_{e_{x,0}}^{\vartheta}$ is the initial value of the Lyapunov function (55). The first time derivative of the sliding surface (54) is given as

$$\dot{s}_{x,1} = k_{x,1} \dot{e}_x + k_{x,2} |e_x|^{\alpha} \operatorname{sign}(e_x). \tag{61}$$

Subsequently, the time derivative of (61) is calculated as

$$\ddot{s}_{x,1} = k_{x,1} \ddot{e}_x - \frac{\alpha k_{x,2}^2}{k_{x,1}} |e_x|^{2\alpha-1} \operatorname{sign}(e_x). \tag{62}$$

Putting (61) and (62) together, the following second-order system is established [46]:

$$\begin{cases} \dot{s}_{x,1} = s_{x,2}, \\ \dot{s}_{x,2} = k_{x,1} \ddot{e}_x - \frac{\alpha k_{x,2}^2}{k_{x,1}} |e_x|^{2\alpha-1} \operatorname{sign}(e_x). \end{cases} \tag{63}$$

Let us define $w_{x,1}$ as

$$w_{x,1} \coloneqq \int s_{x,1} dt. \tag{64}$$

To investigate the stability of the sliding surface $s_{x,1}$, the following Lyapunov function is defined as

$$V_1 \coloneqq \frac{1}{2} s_{x,1}^2 + \frac{\lambda_{x,1}}{2} w_{x,1}^2. \tag{65}$$

Then, the time derivative of V_1 can be obtained as

$$\dot{V}_1 = s_{x,1}\dot{s}_{x,1} + \lambda_{x,1}w_{x,1}\dot{w}_{x,1}, = s_{x,1}s_{x,2} + \lambda_{x,1}w_{x,1}s_{x,1}. \quad (66)$$

The desired $s_{x,2}$, i.e., $s^d_{x,2}$, should be chosen to make $\dot{V}_1$ negative. Thus, from (66), the $s^d_{x,2}$ is given as

$$s^d_{x,2} \coloneqq -\xi_{x,1}s_{x,1} - \lambda_{x,1}w_{x,1}, \quad (67)$$

where $\varphi_{x,1} \coloneqq s^d_{x,2}$ is the virtual variable. The derivative of the virtual control signal $\varphi_{x,1}$, i.e., $\dot{\varphi}_{x,1}$, is required for the controller. Therefore, the problem of "explosion of complexity" should be addressed. For this reason, the following SMBF is employed to estimate $\dot{\varphi}_{x,1}$:

$$\begin{cases} \dot{\varkappa}_{-1} = -\Theta_2 L^{1/3}\lceil \varkappa_{-1}\rfloor^{2/3} + \varkappa_0 - \varphi_{x,1}, \\ \dot{\varkappa}_0 = -\Theta_1 L^{2/3}\lceil \varkappa_{-1}\rfloor^{1/3} + \varkappa_1, \\ \dot{\varkappa}_1 = -\Theta_0 L\lceil \varkappa_{-1}\rfloor^{0}, \end{cases} \quad (68)$$

where $\varkappa_0, \varkappa_1$ are the estimates of $\varphi_{x,1}$ and $\dot{\varphi}_{x,1}$, respectively. Then, the derivative $\dot{\varphi}_{x,1}$ can be accurately restored in a finite time. Hence, $\varkappa_0 \equiv \varphi_{x,1}$ and $\varkappa_1 \equiv \dot{\varphi}_{x,1}$.

Let us define the error between $s_{x,2}$ and $s^d_{x,2}$ as

$$\epsilon_{x,1} \coloneqq s_{x,2} - s^d_{x,2}. \quad (69)$$

Then, equation (69) can be written as

$$s_{x,2} = s^d_{x,2} + \epsilon_{x,1} = -\xi_{x,1}s_{x,1} - \lambda_{x,1}w_{x,1} + \epsilon_{x,1}. \quad (70)$$

Substituting (70) into (66), the time derivative of Lyapunov function V_1 becomes

$$\begin{aligned} \dot{V}_1 &= s_{x,1}(-\xi_{x,1}s_{x,1} - \lambda_{x,1}w_{x,1} + \epsilon_{x,1}) + \lambda_{x,1}w_{x,1}s_{x,1}, \\ &= -\xi_{x,1}s^2_{x,1} + s_{x,1}\epsilon_{x,1}. \end{aligned} \quad (71)$$

Next, we define the integral of the error variable $\epsilon_{x,1}$ as

$$w_{x,2} \coloneqq \int \epsilon_{x,1}dt. \quad (72)$$

To make both the error $\epsilon_{x,1}$ and its integration $w_{x,2}$ converge to zero, the following Lyapunov function candidate is chosen:

$$V_2 \coloneqq V_1 + \frac{1}{2}\epsilon^2_{x,1} + \frac{\lambda_{x,2}}{2}w^2_{x,2}, \quad (73)$$

where $\lambda_{x,2} \in \mathbb{R}_+$. The time derivative of V_2 is given as

$$\dot{V}_2 = \dot{V}_1 + \epsilon_{x,1}\dot{\epsilon}_{x,1} + \lambda_{x,2}w_{x,2}\dot{w}_{x,2}. \quad (74)$$

Using (71) and (72) into (74), it yields

$$\begin{aligned} \dot{V}_2 &= -\xi_{x,1}s^2_{x,1} + s_{x,1}\epsilon_{x,1} + \lambda_{x,2}w_{x,2}\epsilon_{x,1} + \epsilon_{x,1}\dot{\epsilon}_{x,1} \\ &= -\xi_{x,1}s^2_{x,1} + s_{x,1}\epsilon_{x,1} + \lambda_{x,2}w_{x,2}\epsilon_{x,1} \\ &\quad + \epsilon_{x,1}\left[k_{x,1}\ddot{e}_x - \frac{\alpha k^2_{x,2}}{k_{x,1}}|e_x|^{2\alpha-1}\ \text{sign}\ (e_x) - \dot{\varphi}_{x,1}\right]. \end{aligned} \quad (75)$$

Considering $\ddot{e}_x \coloneqq \ddot{x} - \ddot{x}_d$ in (75), it becomes

$$\begin{aligned} \dot{V}_2 &= -\xi_{x,1}s^2_{x,1} + s_{x,1}\epsilon_{x,1} + \lambda_{x,2}w_{x,2}\epsilon_{x,1} \\ &\quad + \epsilon_{x,1}\left[k_{x,1}\left(f_x + F_x + \widehat{d}_x - \ddot{x}_d\right)\right. \\ &\quad \left. - \frac{\alpha k^2_{x,2}}{k_{x,1}}|e_x|^{2\alpha-1}\ \text{sign}\ (e_x) - \dot{\varphi}_{x,1}\right]. \end{aligned} \quad (76)$$

Then, using (76) and taking Assumption 8 into consideration, i.e., $f_x = 0$, the desired virtual controls F^d_x that can stabilize the system is designed as

$$\begin{aligned} F^d_x &\coloneqq -\left(\widehat{d}_x - \ddot{x}_d\right) + \frac{1}{k_{x,1}}\left(\frac{\alpha k^2_{x,2}}{k_{x,1}}|e_x|^{2\alpha-1}\ \text{sign}\ (e_x)\right. \\ &\quad \left. + \dot{\varphi}_{x,1} - \xi_{x,2}\epsilon_{x,1} - s_{x,1} - \lambda_{x,2}w_{x,2}\right). \end{aligned} \quad (77)$$

Remark 16. Many reported works on finite-time control do not provide an estimation of the settling-time. In contrast, we have established rigorous proofs to show that the tracking error dynamics can be stabilized to the origin within a finite bounded time where the upper bound of the convergence time is provided.

Remark 17. In contrast to some reported works on finite-time control, no discontinuous terms appear in the control law (77). The term $|e_x|^{2\alpha-1}\ \text{sign}\ (e_x)$ in the control law is continuous; hence the chattering effect is avoided in the control input. Moreover, to avoid the singularity problem, the fractional exponent $2\alpha - 1$ should be tuned to be greater than 0, i.e., $2\alpha - 1 > 0$. Hence, the parameter α should be chosen to be greater than 0.5, i.e., $\alpha > 0.5$.

Theorem 18. *Given the disturbed translational dynamic model described in (45), the control law designed by (77) can guarantee that the position tracking error e_x is finite-time stable.*

Proof. By substituting the control law designed in (77) into (76), one gets

$$\dot{V}_2 < -\xi_{x,1}s^2_{x,1} - \xi_{x,2}\epsilon^2_{x,1} \le 0. \quad (78)$$

Hence, $\dot{V}_2$ is negative definite, which implies that $s_{x,1}$ and $\epsilon_{x,1}$ will converge to zero equilibrium. Therefore, when the states are confined on the sliding manifold after the reaching phase, it turns that the position error e_x to approach the

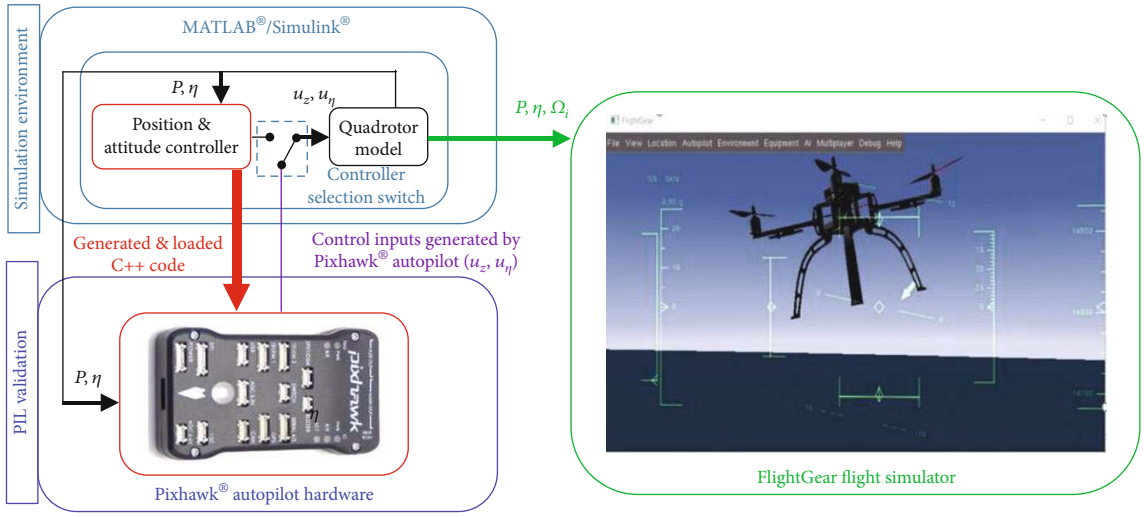

Figure 3: Block diagram of the implementation process from the simulation phase to the real autopilot hardware following an MBD procedure.

origin in a finite time during the sliding phase, i.e., when $s_{x,1} \to 0$ and $\dot{s}_{x,1} \to 0$. This completes the proof.

Remark 19. In the previously reported studies on finite-time control, the sign $(\cdot)$ function appears explicitly in the control law which may cause the chattering and thus making the controller inapplicable in practice. To reduce the chattering effect, some works adopted approximating functions, i.e., sat$(\cdot)$ and tanh $(\cdot)$ functions, to replace the sign $(\cdot)$ function. However, this may degrade and threaten the robustness of the control law leading to a chattering-robustness tradeoff. In contrast to that, no smooth functions are required to approximate the sign $(\cdot)$ function in our control law. Hence, the robustness of the sliding mode is well preserved along with a chattering-free control.

3.2.3. Thrust Force Control and Desired Attitude Computation. The thrust force u_z and the desired attitude angles Φ_d, θ_d are defined in functions of the designed force control $F_P^d := [F_x^d, F_y^d, F_z^d]^T$ for the translational subsystem. The physical meaning of the control vector F_P^d is that it corresponds to the desired forces that make the quadrotor moving along the directions x, y, and z. The thrust force u_z constitutes the magnitude of these forces, whereas their corresponding orientations are determined by the desired attitude $(\chi_7^d = \Phi_d, \chi_9^d = \theta_d, \chi_{11}^d = \psi_d)$, where Φ_d, θ_d, and ψ_d are the desired roll, pitch, and yaw angles, respectively.

Recalling the expressions of $F_P = [F_x, F_y, F_z]^T$ from (47) and combining them with $F_P^d = [F_x^d, F_y^d, F_z^d]^T$, we get

$$\begin{cases} F_x = -u_z m^{-1}\left(c\chi_7^d c\chi_{11}^d s\chi_9^d + s\chi_7^d s\chi_{11}^d\right) := F_x^d, \\ F_y = -u_z m^{-1}\left(c\chi_7^d s\chi_{11}^d s\chi_9^d - c\chi_{11}^d s\chi_7^d\right) := F_y^d, \\ F_z = -u_z m^{-1}\left(c\chi_{11}^d c\chi_9^d\right) + \mathrm{g} := F_z^d. \end{cases} \tag{79}$$

Table 1: Physical parameters of the quadrotor aircraft.

Parameter	Value	Unit
m	1.72	kg
l	0.225	m
g	9.81	m/s^2
J_{xx}	0.0232	kg.m^2
J_{yy}	0.0249	kg.m^2
J_{zz}	0.0342	kg.m^2

Therefore, after some algebraic manipulations of the above expressions, the thrust force u_z and the desired roll and pitch angles $(\chi_7^d = \Phi_d, \chi_9^d = \theta_d)$ for the attitude subsystem can be, respectively, written as

$$\begin{cases} u_z := m\sqrt{\left(F_x^d\right)^2 + \left(F_y^d\right)^2 + \left(F_z^d - \mathrm{g}\right)^2}, \\ \Phi_d := \arcsin\left[-\dfrac{m}{u_z}\left(F_x^d s\psi_d - F_y^d c\psi_d\right)\right], \\ \theta_d := \arctan\left[\dfrac{1}{F_z^d - \mathrm{g}}\left(F_x^d c\psi_d + F_y^d s\psi_d\right)\right]. \end{cases} \tag{80}$$

4. Results and Discussions

To verify the effectiveness of our proposed flight control system, numerical simulations, as well as hardware implementation on a real autopilot, have been conducted. In addition, a comparative study has been carried out. In the following, the software and hardware setup for simulation and implementation is explained.

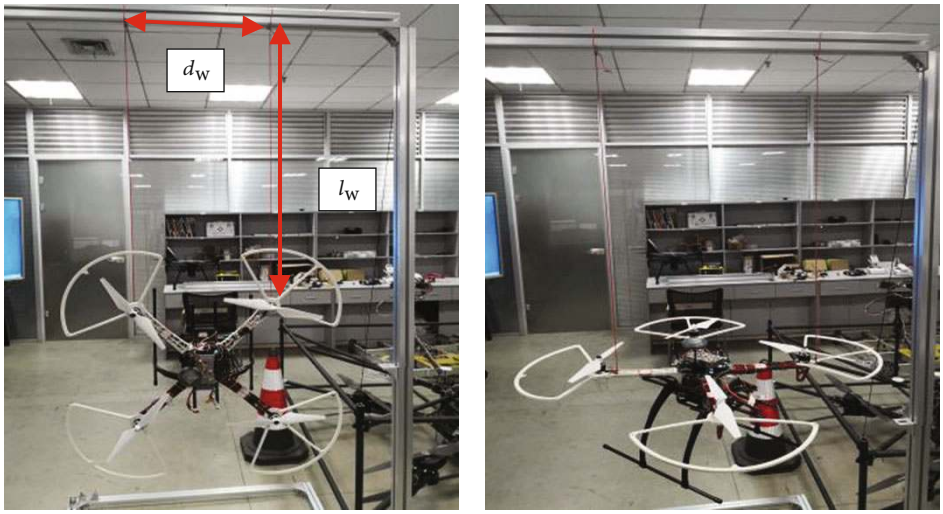

(a) (b)

Figure 4: Bifilar pendulum setup for the estimation of the moments of inertia of the quadrotor: (a) J_{xx} estimation and (b) J_{zz} estimation.

4.1. Software and Hardware Configuration. The procedure that we have followed to verify and implement the proposed control algorithm is known as the model-based design (MBD) framework (see Figure 3) [48]. This procedure is accomplished in two steps. First, the control algorithm is simulated in MATLAB®/Simulink®. Second, the control algorithm is simulated as a C++ code in the real autopilot hardware (PIL simulation). To facilitate the implementation process and conduct the PIL experiment, a specific MATLAB® toolbox called "UAV Toolbox Support Package for PX4® Autopilots" is used. This toolbox allows to automatically generate C++ code for the controller from the MATLAB® code and also to deploy the generated code to the autopilot. This toolbox also allows the communication between the autopilot and Simulink® for data visualization and monitoring by using a USB wire. The control inputs computed by the Pixhawk flight control board are sent back to Simulink® to control the quadrotor model. The hardware set up for the PIL experiment is shown in Figure 1. In both simulation steps (Simulink®, PIL), the position and orientation of the quadrotor are sent to the FlightGear® flight simulator to visualize the flight of the quadrotor in a realistic environment. MATLAB® code and C++ code of the control algorithm are represented by two different blocks in Simulink®. We can switch the choice between these two blocks as can be seen in Figure 3.

The Pixhawk® autopilot includes a main 32-bit STM32F427 system-on-chip, 180 MHz, ARM® Cortex® M4 CPU, 2 MB flash, and 256 KB SRAM with L1 cache. Moreover, STM32F100 value line microcontroller with ARM® Cortex® M3 CPU running on 24 MHz and an SRAM of 8 KB is also included. The processor is running NuttX real-time operating system (RTOS). Besides, the autopilot board includes the following sensors: inertial measurement unit (IMU), Invensense MPU 6000 3-axis accelerometer/gyroscope, ST Micro L3GD20H 16-bit gyroscope, MEAS MS5611 barometer, and ST Micro LSM303D 14-bit accelerometer/magnetometer.

Table 2: Flight control systems compared for the Cartesian trajectory tracking.

Flight control system	Position controller	Attitude controller
FCS 1 (Pixhawk®)	PID	PID
FCS 2 [53]	ANFTSMC	ANFTSMC
FCS 3 [29]	IBSMC	IBSMC
FCS 4 (proposed)	BSITSMC-FXESO	CNTSMC-FTO

Remark 20. Most of the reported works on finite-time control of the quadrotor aircraft may look very promising as evidenced by simulation results. However, owing to lack of practical implementation, their real-world significance may be a valid concern. In contrast, our work presents design, simulation, and hardware realization of modern robust finite-time control laws. The physical implementation in autopilot hardware while attempting to address the above-mentioned problems essentially attributes to the scientific contribution of our work.

4.2. Trajectory Tracking Results and Robustness Test. The numerical simulations and PIL experiments are conducted by using the Euler integration method with a fixed integration step equal to 4×10^{-2} s. The parameters of the quadrotor model are based on a real experimental platform where we have identified them experimentally. These parameters are summarized in Table 1.

We have estimated the moments of inertia (J_{xx}, J_{yy}, J_{zz}) by the bifilar pendulum experiment as shown in Figure 4. The moment of inertia is calculated by (81) as

$$J_{PP} := mgd_w^2 T_{oscil}^2 / 16\pi^2 l_w \left(\text{kg.m}^2\right), \tag{81}$$

where $J_{PP} = \{J_{xx}, J_{yy}, J_{zz}\}$, l_w is the length of the two suspending wires (filars) in meters, d_w is the distance between

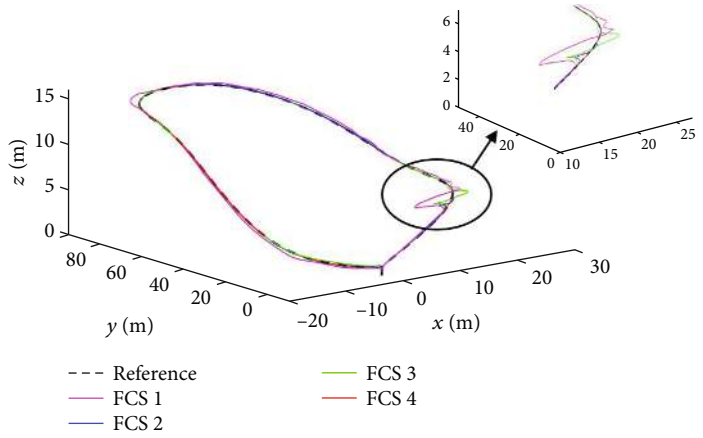

Figure 5: 3D Cartesian flight trajectory tracking for different flight control systems: flight scenario 1.

the two wires in meters, and T_{oscil} is the period of one oscillation in seconds. The period of 10 oscillations is measured using a stopwatch for 5 trials with an initial swing angle equal to 10 degrees. The average value was then used to calculate T_{oscil}.

The parameters of the CNTSMC controller are chosen as $k_1^{\Phi} = k_2^{\Phi} = 10, k_1^{\theta} = k_2^{\theta} = 10, k_1^{\psi} = k_2^{\psi} = 15, \quad \lambda_{\eta} = 3.5, \mu_{\eta} = 12.$ The exponents of the attitude controller are tuned by considering $\bar{\alpha} = 0.85$ and $\xi = 1.5, \varepsilon = 0.001$. The parameters of the FTO observer are set to be $\rho_1^{\eta} = 20, \rho_2^{\eta} = 15, \rho_3^{\eta} = 2, l_{\eta} = 3$. The parameters of the BSITSMC controller are chosen to be $\xi_{i,1} = 0.5, k_{x,1} = 0.25, \xi_{i,2} = 1.2, k_{y,1} = 0.6, ,\lambda_{i,1} = 0.012, k_{z,1} = 0.71, k_{x,2} = 0.15, ,\alpha = 0.8, k_{y,2} = 0.12, \lambda_{i,2} = 0.01, k_{z,2} = 0.2$. The parameters of SMBF are $\Theta_0 = 1.2, \Theta_1 = 1.6, \Theta_2 = 2.5, L = 1.5, r = 3$. Whereas the FXESO observer gains are selected to be $\varepsilon_1 = 0.26, \bar{a} = 0.74, \varepsilon_2 = 0.2, \bar{b} = 1.2, \rho_i^x = \bar{\rho}_i^x = \rho_i^{\Phi} = \bar{\rho}_i^{\Phi} = 5, \rho_i^y = \bar{\rho}_i^y = \rho_i^{\theta} = \bar{\rho}_i^{\theta} = \rho_i^z = 10, \bar{\rho}_i^z = \rho_i^{\psi} = \bar{\rho}_i^{\psi} = 12, l_P = 5$.

To highlight the improvement attained with the proposed control strategy, a comparative study is conducted among four different flight control systems (FCS) (see Table 2). FCS 1 is the default control system of the Pixhawk® autopilot which is based on the PID controller, FCS 2 is based on an adaptive nonsingular fast terminal sliding mode control (ANFTSMC), FCS 3 is based on IBSMC, and FCS 4 is our proposed flight control system.

To better evaluate the FCSs, two different flight scenarios for the Cartesian trajectory tracking are performed. To test the robustness and disturbance rejection capabilities of the FCSs, Cartesian trajectory tracking control has been conducted under the influence of parameter variation and internal model uncertainties as well as external time-varying wind disturbances. This approach is more realistic in practice since all these disturbances and uncertainties are simultaneously present in the dynamic model of the quadrotor. The overall objective is to test the control system in the most complex situation that could be encountered in a real scenario. The total disturbances are given as follows:

(i) External disturbances

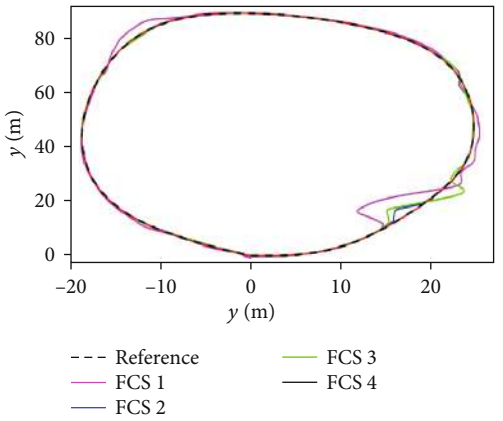

Figure 6: Evolution of the quadrotor's trajectory in 2D ($x - y$ plane) for different flight control systems: flight scenario 1.

Wind disturbances are applied at $t = 15$ s. The disturbances in the position dynamics are generated by the Dryden wind. Their component d_P^{ext} along each axis $P \in \{x, y, z\}$ is expressed as [60]

$$d_P^{\text{ext}}(t) := -k_{d,P}(v_P - v_{w,P})^2 \text{ sign } (v_P - v_{w,P}), \tag{82}$$

and the disturbances on the attitude dynamics are defined by the following expressions:

$$d_{\Phi}^{\text{ext}}(t) = 0.5 \cos(0.4t), d_{\theta}^{\text{ext}}(t) = 0.5 \sin(0.5t), d_{\psi}^{\text{ext}}(t) = 0.5 \sin(0.7t). \tag{83}$$

(ii) Model uncertainties

Considering the simplifications in the Assumption 8 model uncertainties (unmodeled dynamics) are also present as disturbances.

(iii) Parameters' uncertainties

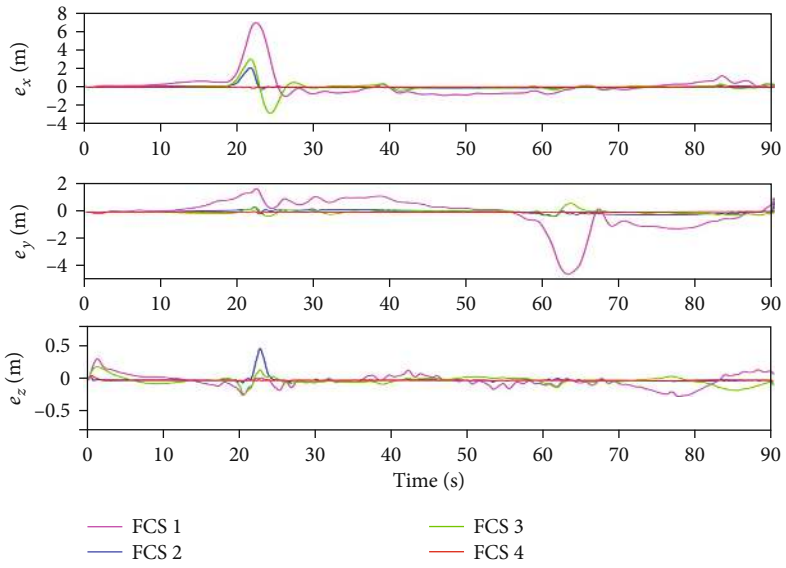

Figure 7: Evolution of the tracking errors for the translational subsystem (e_x, e_y, e_z): flight scenario 1.

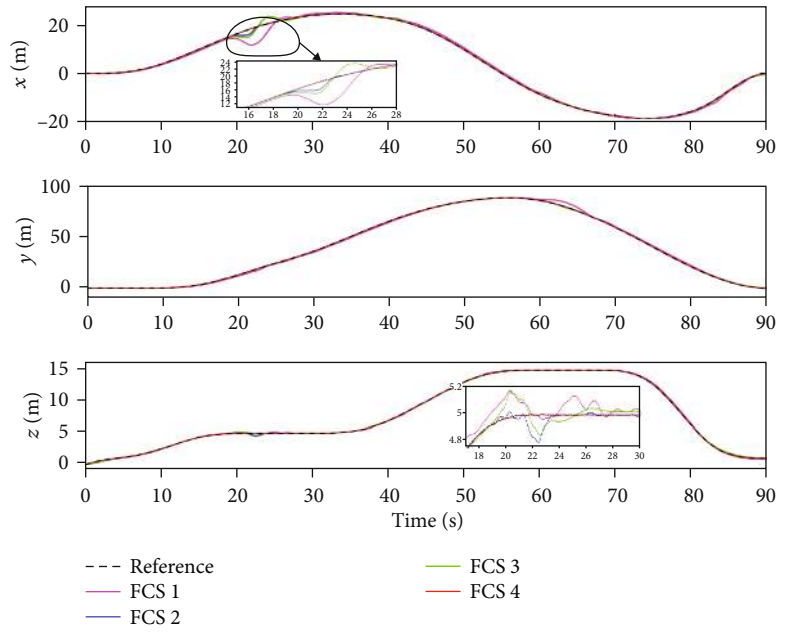

Figure 8: Profiles of the position of the quadrotor: translational variables (x, y, z): flight scenario 1.

Uncertainties of +50% and+30% are introduced in the nominal values of the moments of inertia J_{xx}, J_{yy}, J_{zz}, and the total mass m, respectively.

Furthermore, to make the scenario closer to reality so as to adequately evaluate the control algorithm performance, the measurement noise effects are included while considering the gyroscope sensor data. Also, the measurement errors are added to the data corresponding to GPS and barometer sensors as follows:

(i) Measurement noise

The output of the gyroscope sensor is modeled as

$$\zeta(t) = \tilde{\zeta}(t) + \beta_\zeta + N(t) \ \text{(rad/s)}, \tag{84}$$

where $\zeta = [p, q, r]^T$ rad/s is the final signal used in control, $\tilde{\zeta}$ is the true measurement in rad/s, β_ζ is the measurement bias in rad/s, and $N(t)$ is a random noise with the standard deviation σ_p in rad/s and the mean 0, i.e., $N = \sigma_p$ rand $(\cdot)$, where rand $(\cdot)$ is a MATLAB® function that generates a random number in the interval (0,1).

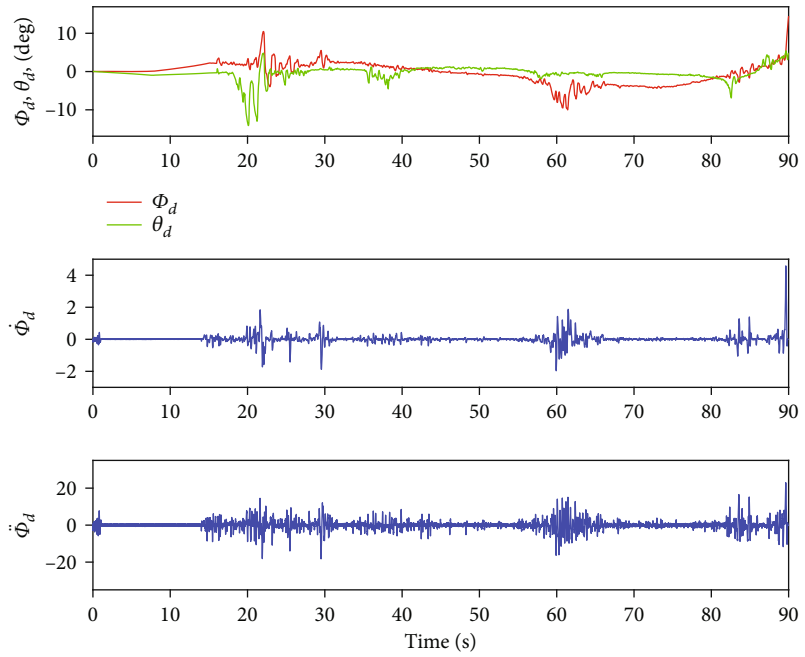

Figure 9: The output signals obtained by REDBTD for the roll angle $(\Phi_d, \dot{\Phi}_d, \ddot{\Phi}_d)$ and pitch angle (θ_d): flight scenario 1.

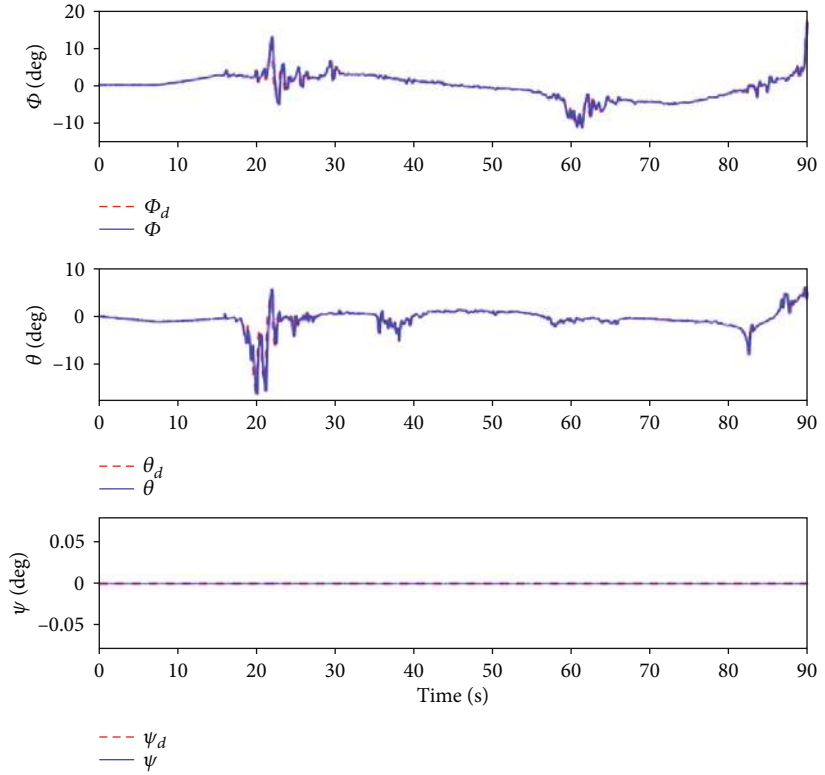

Figure 10: Profiles of the attitude of the quadrotor: Rotational variables (Φ, θ, ψ): flight scenario 1.

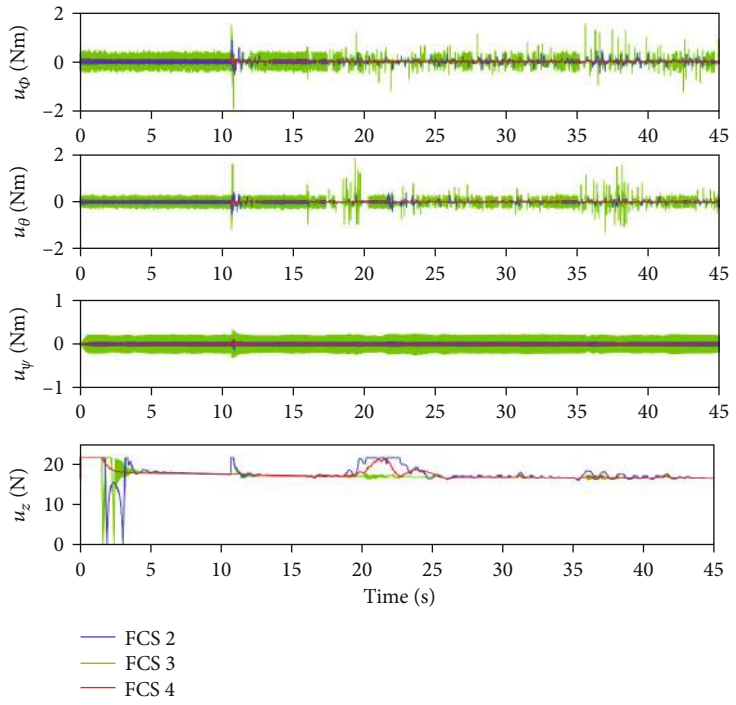

Figure 11: Control signals, i.e., $(u_z, u_\Phi, u_\theta, u_\psi)$, of the proposed FCS 4, FCS 2, and FCS3. The control signals of the proposed FCS 4 are chattering-free: flight scenario 1.

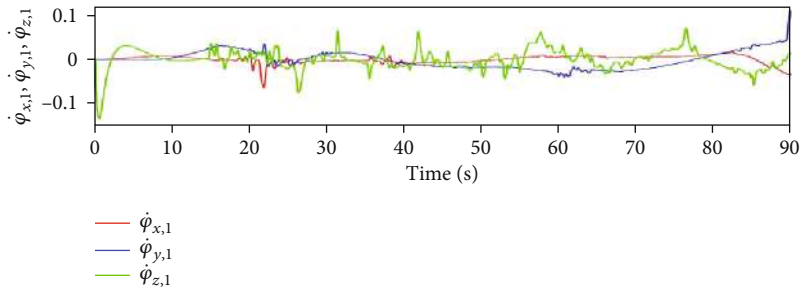

Figure 12: The derivative of virtual law $\dot{\varphi}_{P,1}$ obtained by the SMBF: flight scenario 1.

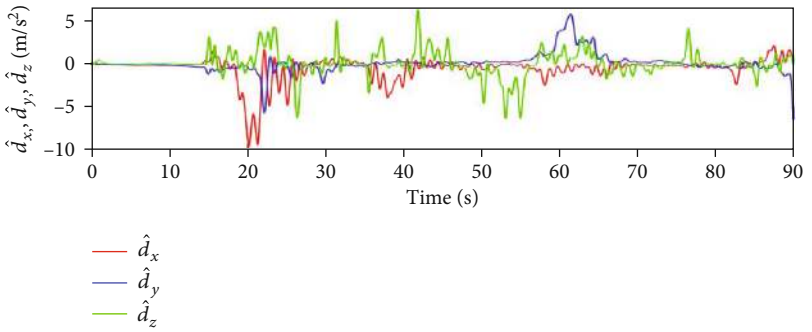

Figure 13: Estimated lumped disturbances for the translational subsystem by the FXESO: flight scenario 1.

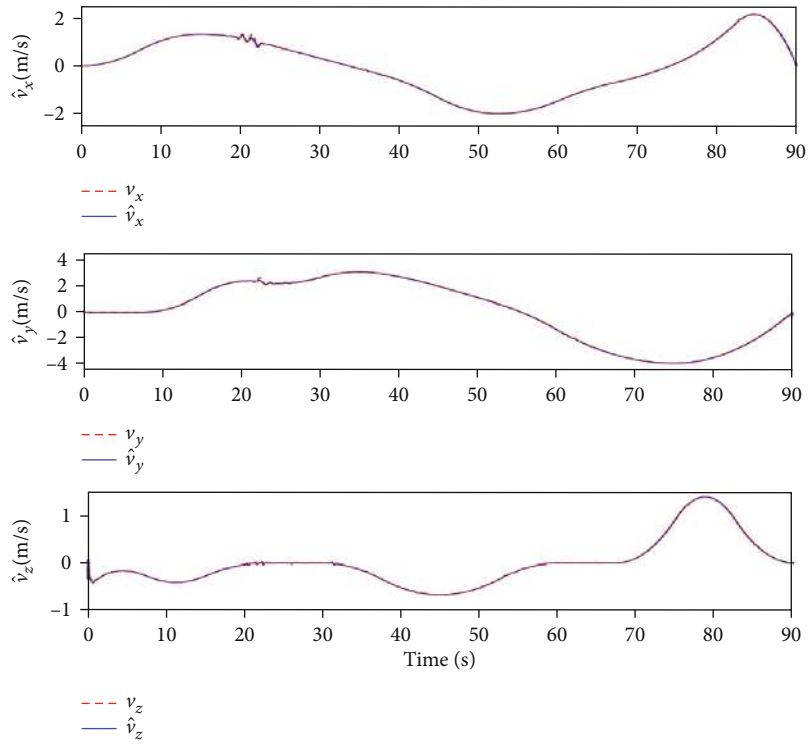

Figure 14: Profiles of the estimated velocities of the quadrotor $(\hat{v}_x, \hat{v}_y, \hat{v}_z)$ by the FXESO observer: flight scenario 1.

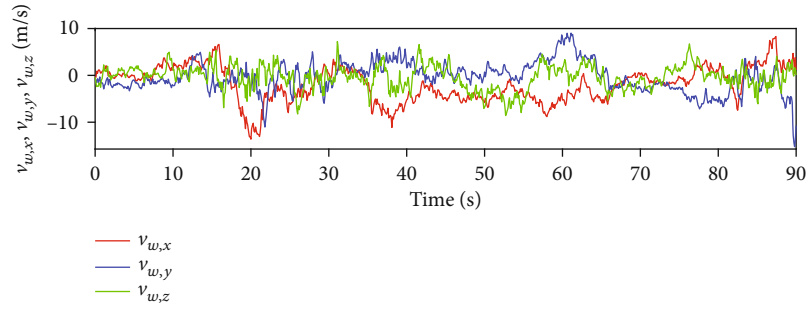

Figure 15: Velocities of the simulated Dryden wind.

(ii) Position error

The GPS and barometer signals are obtained as

$$P(t) = \tilde{P}(t) + \text{rand}\,(\cdot)P_e\,(\text{m}), \tag{85}$$

where $\tilde{P}$ is the true measurement and P_e is the position error.

4.2.1. Flight Scenario 1. For this trajectory tracking scenario, we consider a practical and more realistic example. The quadrotor is required to accomplish a flight mission by following a set of waypoints listed in the form of (x_{wp}, y_{wp}, z_{wp}) triples as follows: (0,0,0), (0,0,1), (0,0,1), (10,0,5), (20,20,5), (25,35,5), (25,60,5), (20,80,10), (5,90,15), (-10,90,15), (-17,70,15), (-20,40,15), (-15,10,1), (0,0,1), (0,0,1). In practice, these waypoints can be set manually or can be generated by a specific path planning algorithm such as the well-known rapidly exploring random tree (RRT) algorithm [8] or A* Algorithm [61]. The B-spline polynomial algorithm is used to generate a dynamically feasible and smooth Cartesian trajectory that passes through the given waypoints. The initial conditions of the quadrotor's states are $P_0 = [x_0, y_0, z_0]^T = [0, 0, 0]^T$ m, $\eta_0 = [\Phi_0, \theta_0, \psi_0]^T = [0, 0, 0]^T$ deg.

The results of the PIL simulation for the trajectory tracking are presented in Figures 5–16. The way in which the aircraft follows the reference flight trajectory for the different control methods is presented in the 3D space in Figure 5. The evolution of the quadrotor's trajectory in the $x - y$ plane is presented in Figure 6. The first observation from Figures 5 and 6 is that all the controllers can track the reference trajectory. However, it is clear that the PID controller is affected by the disturbances. The position tracking errors are displayed in Figure 7, whereas the actual and desired positions are

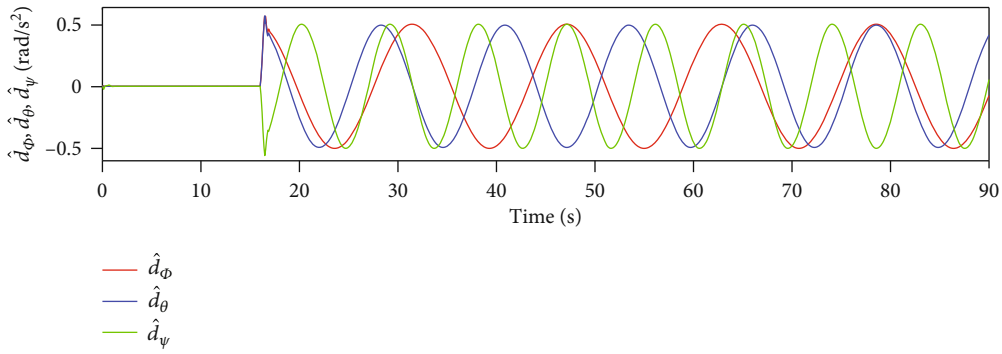

Figure 16: Estimated lumped disturbances for the rotational subsystem by the FTO observer.

Table 3: ISE performance index analysis: flight scenario 1.

Control strategy	Performance index ISE		
	x	y	z
FCS 1 (Pixhawk®)	172.5	28.47	0.83
FCS 2 [53]	6.02	1.39	0.05
FCS 3 [29]	28.32	1.47	0.32
FCS 4 (proposed)	0.10	0.22	0.003

Table 4: IADU performance index for chattering analysis.

Control strategy	Performance index IADU			
	u_z	u_Φ	u_θ	u_ψ
FCS 3 [29]	0.108	0.0805	0.122	0.996
FCS 2 [53]	0.037	0.010	0.031	0.03
FCS 4 (proposed)	0.029	0.006	0.010	0.007

shown in Figure 8. It can be seen from Figure 7 that all the controllers successfully converged the translational variables to the required set-points in the presence of the abruptly changing reference. However, a closer inspection of the tracking errors in Figure 7 shows that the proposed control method is more accurate regarding the reference trajectory tracking on the x, y, and z axes as compared to the other controllers. It can be seen that the tracking errors converge to the origin and continue staying in the vicinity of the origin. All the controllers are affected by the wind gust at $t = 20$s for the position x and at $t = 22$s for the position y except our proposed controller, which exhibits an effective disturbance rejection capability. This enhanced robustness in our suggested FCS is due to the adopted TSMBAADC control strategy including the robust ADRC and the DOBC control structures based on the nonlinear terminal SMC. It is evident that the PID controller is more sensitive to disturbances and suffers from a lack of robustness with large tracking errors. This is because the control law of the PID does not consider the quadrotor's dynamics. Also, we can see that the FCS 2 which is based on the ANFTSMC provides noticeable disturbance rejection.

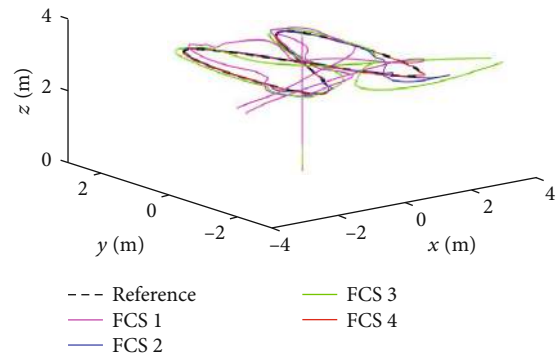

Figure 17: 3D Cartesian flight trajectory tracking for different flight control systems: flight scenario 2.

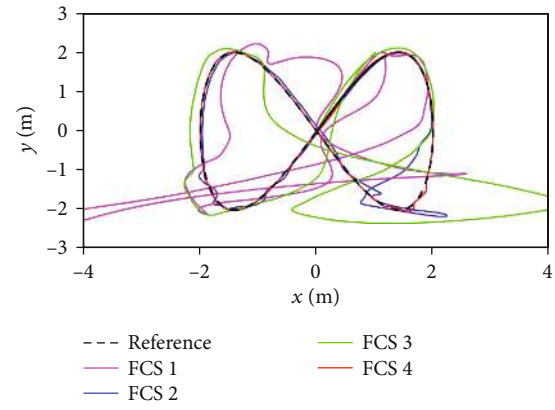

Figure 18: Evolution of the quadrotor's trajectory in 2D ($x - y$ plane) for different flight control systems: flight scenario 2.

To provide a more precise quantitative comparison of the achieved results, the integral of square error (ISE) index is used for error signal analysis. The ISE is defined as

$$\text{ISE} = \int_{t_0}^{t_f} e_P(\tau)^2 d\tau, \tag{86}$$

where $P = \{x, y, z\}$. This performance index is computed and summarized in Table 3 where the best performances are shown in boldface.

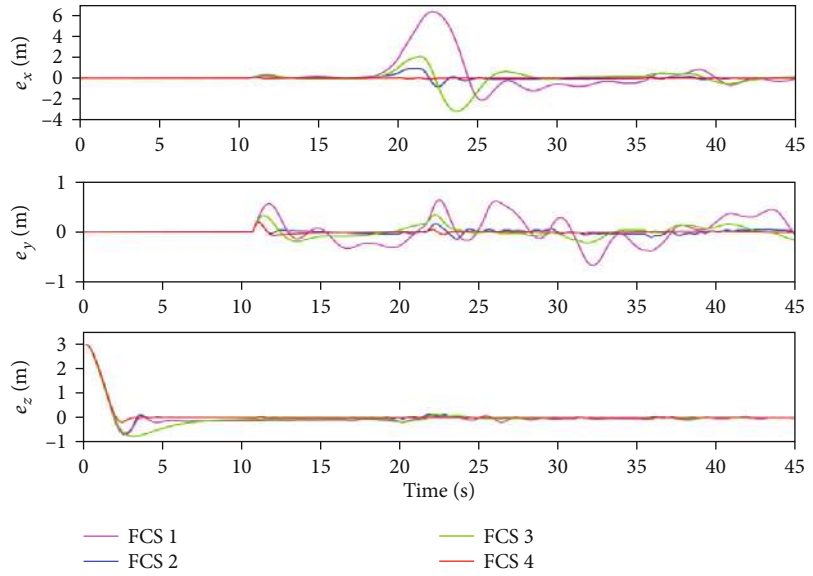

Figure 19: Evolution of the tracking errors for the translational subsystem (e_x, e_y, e_z): flight scenario 2.

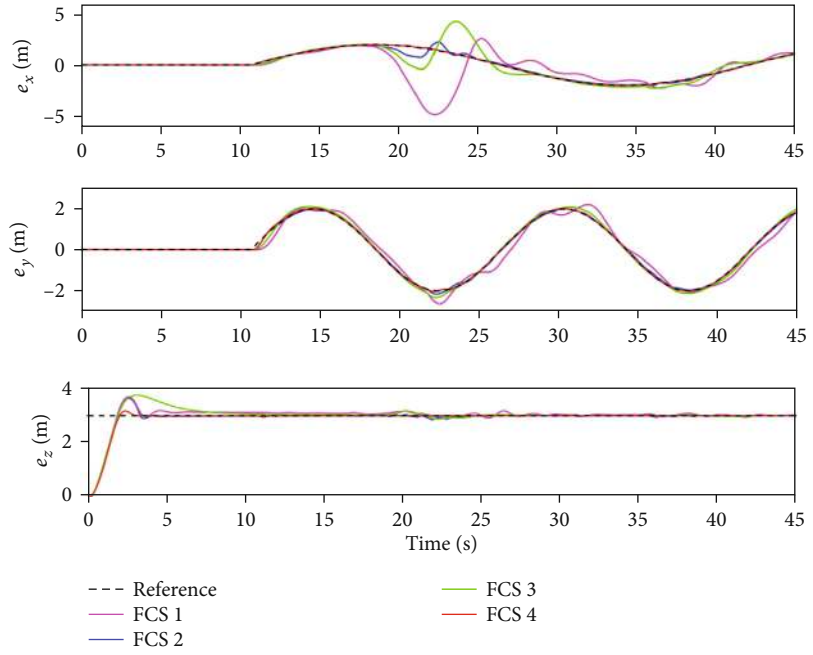

Figure 20: Profiles of the position of the quadrotor: translational variables (x, y, z): flight scenario 2.

We can see from Table 3 that the proposed control strategy has the smallest ISE index for the x, y, and z states. The PID controller is observed to have the largest ISE index. This can be explained by the fact that the proposed FCS has a strong disturbance rejection feature which leads to enhancing the robustness.

Meanwhile, the desired attitude signals, their first and second derivative provided by the REDBTD, are depicted in Figure 9. It is clear that the REDBTD can provide a continuous, smooth, and bounded estimate of the desired attitude signal and its derivative. Such that the high frequency due to the traditional differentiation can be filtered out.

The attitude tracking of the proposed robust CNTSMC controller is shown in Figure 10. It can be observed that the proposed attitude controller guarantees a robust and accurate tracking of the attitude reference. The control signals for the SMC-based controllers, i.e., IBSMC, ANFTSMC, and the proposed controller are depicted in Figure 11 where we can see that the magnitudes of the inputs are within the admissible ranges in the case of the proposed controller. Moreover, unlike the IBSMC that is affected by chattering, the control inputs of the proposed control system have no chattering effect. We can also observe that the FCS2 which is based on the ANFTSMC controller allows mitigating the chattering

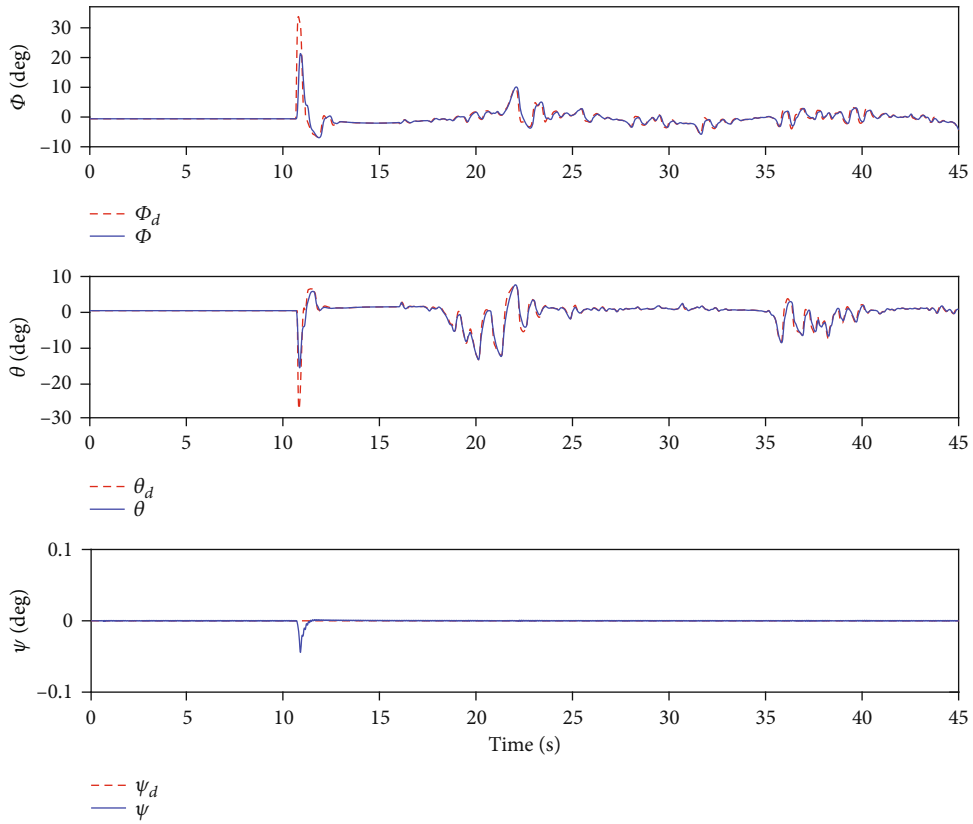

Figure 21: Profiles of the attitude of the quadrotor: rotational variables (Φ, θ, ψ): flight scenario 2.

effect; however, our proposed controller has the overall superiority since the control signals provided by the control law are continuous.

The well-known integral of the absolute value of the derivative of the input $u(t)$ (IADU) criterion is used for the control signal (shown in Figure 11) analysis. It is given as

$$\text{IADU} = \int_{t_i}^{t_f} \left| \frac{du(\tau)}{d\tau} \right| d\tau. \tag{87}$$

The IADU index is very appropriate to check the control signal smoothness and thereby indicates chattering alleviation capability for the control input [62]. Taken together, the control signal results are compared in Table 4.

It is apparent from this table that the smoothness is improved by the proposed control strategy for all control signals compared to the IBSMC and ANFTSMC controllers. Thus, the chattering effect has been effectively alleviated.

The output $\dot{\varphi}_{i,1}$ of the SMBF which is employed to tackle the "explosion of complexity" issue is shown in Figure 12. It is evident that the filter provides a bounded and smooth estimate of the virtual control signal. We can see that the output signal provided by the differentiator is not affected by the noise; hence, the controller is more applicable in practice.

Figures 13 and 14 display the outputs provided by the designed FXESO observer. Figure 13 shows the estimated lumped disturbances along the three axes. It can be observed that the disturbances can be exactly estimated along the three axes after they have been applied to the quadrotor system at $t = 15$s, which leads to enhancing the robustness of the control system against strong lumped disturbances. The estimates of the velocities are presented in Figure 14 from which it is clear that the FXESO observer provides a precise velocity estimate within a very short convergence time. By estimating the velocities, the velocity-free control can be achieved where only the position of the quadrotor is assumed to be measurable. This prominent result of the adopted output-feedback control contributes to avoiding the shortcoming of the full-state feedback-based controllers. Thus, the proposed control method relying on velocity-free control is robust against the accelerometer's faults.

Figure 15 depicts the velocities of the simulated Dryden wind, from which it can be seen that the wind gusts can reach a speed of around 10 m/s and 15 m/s, which is a challenging flight condition for the FCS. The estimated lumped disturbances affecting the rotational subsystem are presented in Figure 16. The designed FTO observer allows estimating the disturbances accurately within a fast convergence time, which improves the robustness of the attitude controller and thus leading to precise tracking of the attitude reference.

4.2.2. Flight Scenario 2. The quadrotor is required to track the following time-varying Cartesian trajectory:

$$[x_d, y_d, z_d, \psi_d]^T = [2 \sin(0.2t), 2 \sin(0.2t) \cos(0.2t), 3, 0]^T. \tag{88}$$

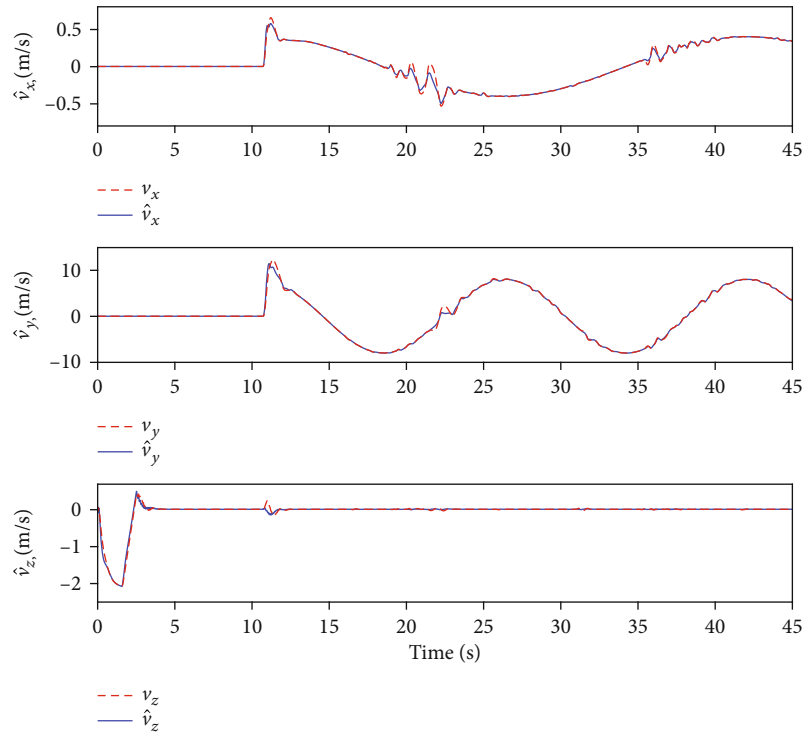

Figure 22: Profiles of the estimated velocities of the quadrotor $(\hat{v}_x, \hat{v}_y, \hat{v}_z)$ by the FXESO observer: flight scenario 2.

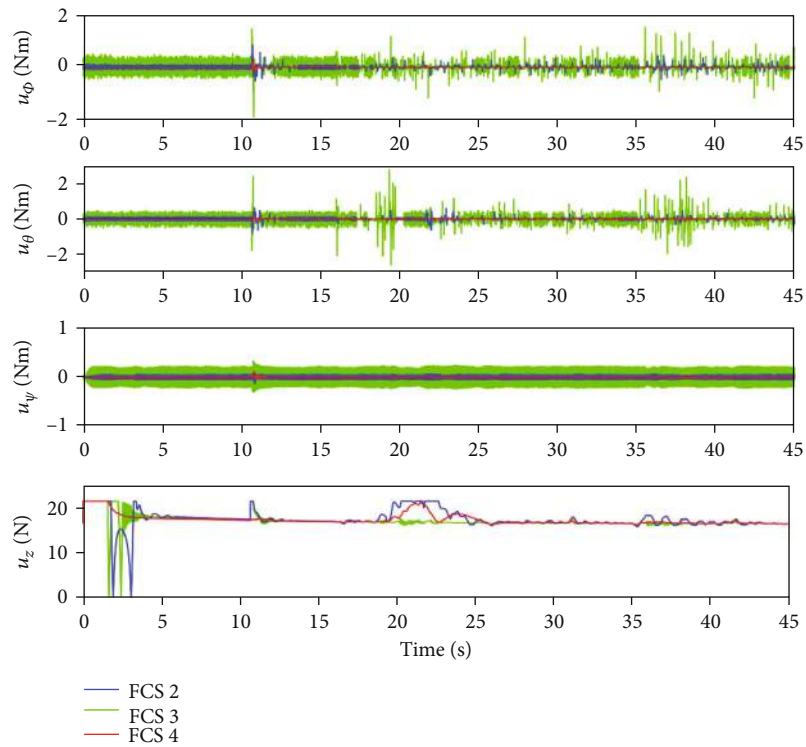

Figure 23: Control signals, i.e., $(u_z, u_\Phi, u_\theta, u_\psi)$, of the proposed FCS 4, FCS 2, and FCS3. The control signals of the proposed FCS 4 are chattering-free: flight scenario 2.

Table 5: ISE performance index analysis: flight scenario 2.

Control strategy	Performance index ISE		
	x	y	z
FCS 1 (Pixhawk®)	50.41	15.20	10.83
FCS 2 [53]	8.12	2.39	8.31
FCS 3 [29]	16.27	4.47	9.14
FCS 4 (proposed)	0.25	0.27	7.96

The results of this flight scenario are presented in Figures 17–23. The 3D trajectory tracking for different FCSs is presented in Figure 17, and the evolution of the quadrotor's trajectory in the $x - y$ plane is given in Figure 18. The profiles of the tracking errors and the translational variables are depicted in Figures 19 and 20, respectively. It can be seen from these figures that the designed FCS succeeds in tracking the desired flight trajectory with high accuracy while external disturbances, parameter variation, and model uncertainty effects are well compensated. Figure 21 presents the profiles of the rotational variables of the quadrotor (Φ, θ, ψ). As in the first flight scenario, the proposed attitude controller ensures precise tracking of the three angles. The signals of the unmeasurable states of the quadrotor are successfully and accurately estimated by the designed FXESO observer as is shown in Figure 22. From Figure 23, we can see again that the control inputs provided by our suggested FCS are chattering-free and are within the admissible range.

The results obtained from the analysis of tracking errors using the ISE index are compared in Table 5. The best performances are shown in bold text. Similar to the previous flight scenario, the obtained results confirm the effectiveness of the proposed FCS in dealing with trajectory tracking even in the presence of fast-time varying external disturbances and model uncertainties. Moreover, the proposed FCS demonstrates the superior performance w.r.t the employed performance index related to the position tracking errors.

5. Conclusion

This research work presents a solution to the robust finite-time trajectory tracking control problem of a quadrotor system subjected to various disturbances. A new FCS has been proposed. The design of the control laws is based on two steps: attitude control design and position control design. First, a robust DOBC has been constructed to stabilize the inner attitude loop. In addition, a REDBTD has been introduced to supply smooth and bounded attitude reference signals. Second, an ADRC approach has been proposed by creatively combining a BSITSMC strategy and an FXESO observer. Besides, the "explosion of complexity" problem in BS design has been addressed by designing an SMBF. The most distinguishing feature of the proposed FCS lies in its ability to track the trajectory in finite-time under lumped disturbances. The control law is smooth without undesirable singularity or chattering effect. Stability analysis for the closed-loop system has been provided based on the Lyapunov theorem. PIL implementations on real Pixhawk® autopilot have corroborated the theoretical findings. Furthermore, a comparative study has been made with relevant works to evaluate the performance and show the improvements attained by the developed flight controller. The obtained results confirm the superiority of the proposed control strategy regarding the accuracy, robustness, and chattering alleviation.

As an extension and improvement to the present study, fixed-time stability could be addressed in our future works. Fixed-time stability is aimed at predefining and adjusting a uniformly bounded settling time. Such a control method allows for stabilizing the system's states in a fixed time independently of initial conditions. This important property is potentially useful in practical scenarios of the quadrotor since it enhances the system's robustness and provides faster convergence. Besides, this interesting feature is pivotal in the cooperative control of the multiquadrotor systems, which lies in our research. Also, actuator faults and control input saturation are interesting aspects that could also be addressed. In addition, an optimization method could be usefully introduced for the tuning of the control parameters. Finally, a real outdoor flight experiment could be conducted to further evaluate the proposed flight-control system.

Nomenclature

$\mathbb{R}$:	Set of real numbers
$\mathbb{R}^n$:	n-dimensional state-space
$\mathbb{R}_+ \coloneqq \{x \in \mathbb{R} : x \geq 0\}$:	Set of positive real numbers
$\dot{x}, \ddot{x}$:	First and second-time derivatives of a variable x
$\lvert x \rvert$:	Absolute value of x in $\mathbb{R}$
$\lceil x \rfloor^{\alpha}$:	$\lceil x \rfloor^{\alpha} \coloneqq \lvert x \rvert^{\alpha} \operatorname{sign}(x) \forall x \in \mathbb{R}$ and $\alpha \in \mathbb{R}_+$
sign $(\cdot)$:	Standard signum function
$\mathscr{C}^1$:	Class $\mathscr{C}^1$ is the space of continuously differentiable functions
t, τ, t_i, t_f:	Time variables
$i = \overline{1, n}$:	Sequence of integers $i = 1, \cdots, n$
$\lambda_{\min}(A), \lambda_{\max}(A)$:	Minimum and maximum eigenvalue of matrix A
diag $(a_1, a_2, \cdots, a_n) a_n \in \mathbb{R}$:	Diagonal matrix
sx, cx:	sin x, cos x
$P = [x, y, z]^T$:	Position of the aircraft in the E-frame
$B = (\mathcal{O}_B, \mathrm{x}_B, \mathrm{y}_B, \mathrm{z}_B)$:	Body-fixed frame "B-frame"
$E = (\mathcal{O}_E, \mathrm{x}_E, \mathrm{y}_E, \mathrm{z}_E)$:	Earth-fixed frame "E-frame" (inertial frame)
$\eta = [\Phi, \theta, \psi]^T$:	Euler angles in B-frame (roll, pitch, yaw)
$Y \coloneqq [\dot{x}, \dot{y}, \dot{z}]^T = [v_x, v_y, v_z]^T$:	Velocity of the aircraft in E-frame
$\zeta \coloneqq [p, q, r]^T$:	Angular velocities of the aircraft
m:	Total mass of the quadrotor

l: Length of the quadrotor's arm

$d_P \coloneqq [d_x, d_y, d_z]^T$: Total disturbances acting on the quadrotor

$d_\eta \coloneqq [d_\Phi, d_\theta, d_\psi]^T$:

$f_i \in \mathbb{R}_+, (i = \overline{1,4})$: Forces produced by each rotor

$d_\eta^{\text{unc}}, d_P^{\text{unc}}$: Unmodeled dynamics and uncertainties

$d_\eta^{\text{ext}}, d_P^{\text{ext}}$: External disturbances

g: Gravitational acceleration constant

$K_a \coloneqq \text{diag}\,(k_x, k_y, k_z)$: Diagonal aerodynamic drag matrix

$u_\eta \coloneqq [u_\Phi, u_\theta, u_\psi]^T$: Control inputs for the attitude subsystem

u_z: Thrust control (total lift force)

J_r: Inertia of the rotor

$J \coloneqq \text{diag}\,(J_{xx}, J_{yy}, J_{zz})$: Moments of inertia matrix

$\Omega_i, (i = \overline{1,4})$: Angular speed of the rotors

$\mathscr{c}_\Phi, \mathscr{c}_\theta, \mathscr{c}_\psi \in \mathbb{R}_+$: Aerodynamic friction coefficients

$\mathscr{c}_d, \mathscr{c}_t \in \mathbb{R}_+$: Drag coefficient and thrust coefficient

$k_{d,P} \in \mathbb{R}_+$: Positive constant

$v_P, v_{w,P}, P = \{x, y, z\}$: Quadrotor's and wind's velocities

l_η, l_P: Upper bound of $\|\dot{d}_\eta\|$ and $\|\dot{d}_P\|$

τ_a, τ_g: Aerodynamic and gyroscopic moments

F_a: Drag force

$\bar{\omega}$: $\bar{\omega} \coloneqq \Omega_1 - \Omega_2 + \Omega_3 - \Omega_4$ is the overall residual angular velocity of the rotor

$\varkappa$: Variable of the tracking differentiator (TD)

$k_0, k_1, k_2 \in \mathbb{R}_+$: Constant parameters of the TD

$\chi, \bar{\mathrm{x}}, X_\eta, X_P$: State vectors

f_η, g_η, f_P, F_P: Smooth vector fields

$\mathscr{Y}_1 = [\Phi, \theta, \psi]^T, \mathscr{Y}_2 = [x, y, z]^T$: Vectors of the controlled outputs

$\rho_1^\eta, \rho_2^\eta, \rho_3^\eta \in \mathbb{R}_+$: Constants for the FTO observer design

$\rho_1^P, \rho_2^P, \rho_3^P, \bar{\rho}_1^P, \bar{\rho}_2^P, \bar{\rho}_3^P \in \mathbb{R}_+$: Constants for the FXESO observer design

$?_0, ?_1$: Intermediate variables for the FTO observer design

Γ_2^η: Estimates of d_η

$\Gamma_1^P, \Gamma_2^P, \Gamma_3^P$: Estimates of P, Y, and d_P

$\ell_1^\eta, \ell_2^\eta, \ell_3^\eta$: Observation errors of the FTO observer

$\ell_1^P, \ell_2^P, \ell_3^P$: Observation errors of the FXESO observer

$h, \delta \in \mathbb{R}_+$: Positive constants

Q_1, Q_2, P_1, P_2: Nonsingular, symmetric, and positive-definite matrices

$e_1^\eta \coloneqq e_\eta$ and $e_2^\eta \coloneqq \dot{e}_\eta$: Attitude tracking error and its dynamics

$s_\eta, s_{x,1}, s_{x,2}$: Sliding surfaces

$\lambda_\eta, \mu_\eta, k_j^\eta \in \mathbb{R}_+$.: Positive parameters

$k_{x,1}, k_{x,2}, \varsigma, \vartheta, \lambda_{x,1}, \xi_{x,1} \in \mathbb{R}_+$: Positive parameters

$\xi, \varepsilon, \alpha, \alpha_{1,j}, \alpha_{2,j} (j = \overline{1,2})$: Positive exponents

u_{eq_η}, u_{r_η}: Equivalent control and reaching control

$\widehat{d}_\eta, \widehat{d}_P$: Estimates of d_η and d_P, respectively

V: Positive-definite Lyapunov function

$T_r, T^\star$: Reaching time during the sliding motion and its upper bound

T_0, T_2: Convergence time of the FTO and FXESO observers

T_1, T_3: Convergence time of attitude and position tracking errors

e_x: Tracking error for x position

$w_{x,1}, w_{x,2}, \epsilon_{x,1}$: Control design variables

$\varphi_{x,1}$: Virtual control signal

$\Theta_0, \Theta_1, \Theta_2, L$: Positive parameters of SMBF

$\varkappa_0, \varkappa_1$: Estimates of $\varphi_{x,1}$ and $\dot{\varphi}_{x,1}$.

Data Availability

The data used to support the findings of this study are available from the corresponding author upon request.

Conflicts of Interest

The authors declare that there is no conflict of interest regarding the publication of this paper.

Acknowledgments

This work was supported by the National Natural Science Foundation of China under Grant No. 61803075 and the Fundamental Research Funds for the Central Universities under Grants No. ZYGX2018KYQD211 and No. ZYGX2019J084.

References

[1] S. G. Khan, S. Bendoukha, W. Naeem, and J. Iqbal, "Experimental validation of an integral sliding mode-based LQG for the pitch control of a UAV-mimicking platform," *Advances in Electrical and Electronic Engineering*, vol. 17, no. 3, pp. 275–284, 2019.

[2] A. Tayebi and S. McGilvray, "Attitude stabilization of a four-rotor aerial robot," in *2004 43rd IEEE Conference on Decision*

and Control (CDC) (IEEE Cat. No.04CH37601), vol. 2, pp. 1216–1221, Nassau, Bahamas, 2004.

[3] S. Ullah, Q. Khan, A. Mehmood, S. A. M. Kirmani, and O. Mechali, "Neuro-adaptive fast integral terminal sliding mode control design with variable gain robust exact differentiator for under-actuated quadcopter UAV," *ISA Transactions*, 2021, In Press.

[4] X. Liang, Y. Fang, N. Sun, and H. Lin, "Dynamics analysis and time-optimal motion planning for unmanned quadrotor transportation systems," *Mechatronics*, vol. 50, pp. 16–29, 2018.

[5] C. Sampedro, A. Rodriguez-Ramos, H. Bavle, A. Carrio, P. de la Puente, and P. Campoy, "A fully-autonomous aerial robot for search and rescue applications in indoor environments using learning-based techniques," *Journal of Intelligent & Robotic Systems*, vol. 95, no. 2, pp. 601–627, 2019.

[6] S. Sudhakar, V. Vijayakumar, C. Sathiya Kumar, V. Priya, L. Ravi, and V. Subramaniyaswamy, "Unmanned aerial vehicle (UAV) based forest fire detection and monitoring for reducing false alarms in forest-fires," *Computer Communications*, vol. 149, pp. 1–16, 2020.

[7] G. Fan, W. Mingzhu, Y. Mingfei, L. Jiajun, O. Mechali, and Y. Cao, "An unmanned aerial vehicles collaborative searching and tracking scheme in three-dimension space," in *2019 IEEE 9th Annual International Conference on CYBER Technology in Automation, Control, and Intelligent Systems (CYBER)*, pp. 1262–1266, Suzhou, China, 2019.

[8] O. Mechali, L. Xu, M. Wei, F. Guo, and A. Senouci, "A rectified RRT∗ with efficient obstacles avoidance method for UAV in 3D environment," in *2019 IEEE 9th Annual International Conference on CYBER Technology in Automation, Control, and Intelligent Systems (CYBER)*, pp. 480–485, Suzhou, China, 2019.

[9] S. Ullah, A. Mehmood, Q. Khan, S. Rehman, and J. Iqbal, "Robust integral sliding mode control design for stability enhancement of underactuated quadcopter," *International Journal of Control, Automation and Systems*, vol. 18, no. 7, pp. 1671–1678, 2020.

[10] M. Wasim, M. Ullah, and J. Iqbal, "Gain-scheduled proportional integral derivative control of taxi model of unmanned aerial vehicles," *Revue Roumaine des Sciences Techniques-Serie Electrotechnique et Energetique*, vol. 64, no. 1, pp. 75–80, 2019.

[11] A. Roberts and A. Tayebi, "Adaptive position tracking of VTOL UAVs," *IEEE Transactions on Robotics*, vol. 27, no. 1, pp. 129–142, 2011.

[12] K. Eliker, S. Grouni, M. Tadjine, and W. Zhang, "Practical finite time adaptive robust flight control system for quadcopter UAVs," *Aerospace Science and Technology*, vol. 98, article 105708, 2020.

[13] X. Ai and J. Yu, "Fixed-time trajectory tracking for a quadrotor with external disturbances: a flatness-based sliding mode control approach," *Aerospace Science and Technology*, vol. 89, pp. 58–76, 2019.

[14] S. Bouabdallah, A. Noth, and R. Siegwart, "PID vs LQ control techniques applied to an indoor micro quadrotor," in *International Conference on Intelligent Robots and Systems (IROS)*, vol. 3, pp. 2451–2456, Sendai, Japan, 2004.

[15] M. Bouchoucha, M. Tadjine, A. Tayebi, and P. Mullhaupt, "Backstepping based nonlinear PI for attitude stabilisation of a quadrotor: from theory to experiment," in *2008 IEEE/RSJ International Conference on Intelligent Robots and Systems*, pp. 4183–4183, Nice, France, 2008.

[16] A. Tayebi and S. McGilvray, "Attitude stabilization of a VTOL quadrotor aircraft," *IEEE Transactions on Control Systems Technology*, vol. 14, no. 3, pp. 562–571, 2006.

[17] S. Khatoon, D. Gupta, and L. K. Das, "PID & LQR control for a quadrotor: modeling and simulation," in *2014 International Conference on Advances in Computing, Communications and Informatics (ICACCI)*, pp. 796–802, Delhi, India, 2014.

[18] L. M. Argentim, W. C. Rezende, P. E. Santos, and R. A. Aguiar, "PID, LQR and LQR-PID on a quadcopter platform," in *2013 International Conference on Informatics, Electronics and Vision (ICIEV)*, pp. 1–6, Dhaka, Bangladesh, 2013.

[19] J. Zhang, D. Gu, Z. Ren, and B. Wen, "Robust trajectory tracking controller for quadrotor helicopter based on a novel composite control scheme," *Aerospace Science and Technology*, vol. 85, pp. 199–215, 2019.

[20] J. Liu, W. Gai, J. Zhang, and Y. Li, "Nonlinear adaptive backstepping with ESO for the quadrotor trajectory tracking control in the multiple disturbances," *International Journal of Control, Automation and Systems*, vol. 17, no. 11, pp. 2754–2768, 2019.

[21] M. Labbadi and M. Cherkaoui, "Robust adaptive backstepping fast terminal sliding mode controller for uncertain quadrotor UAV," *Aerospace Science and Technology*, vol. 93, article 105306, 2019.

[22] T. Jiang, D. Lin, and T. Song, "Finite-time backstepping control for quadrotors with disturbances and input constraints," *IEEE Access*, vol. 6, pp. 62037–62049, 2018.

[23] Y. Liu, L. Huang, and D. Xiao, "Adaptive dynamic surface control for uncertain nonaffine nonlinear systems," *International Journal of Robust and Nonlinear Control*, vol. 27, no. 4, pp. 535–546, 2017.

[24] D. J. Almakhles, "Robust backstepping sliding mode control for a quadrotor trajectory tracking application," *IEEE Access*, vol. 8, pp. 5515–5525, 2020.

[25] S. T. F. Mobayen and F. Tchier, "Nonsingular fast terminal sliding-mode stabilizer for a class of uncertain nonlinear systems based on disturbance observer," *Scientia Iranica*, vol. 24, no. 3, pp. 1410–1418, 2016.

[26] O. Mechali, *Commande non-linéaire robuste sans capteur de la machine MSAP, 17 meldrum street, beau bassin 71504, mauritius*, Edition Universités Européennes, 2019.

[27] O. Mechali, L. Xu, A. Senouci, X. Xie, C. Xin, and A. Mechali, "Finite-time observer-based robust continuous twisting control for the attitude of an uncertain quadrotor UAV subjected to disturbances," in *2020 IEEE International Conference on Mechatronics and Automation (ICMA)*, pp. 1203–1208, Beijing, China, 2020.

[28] E. Kayacan, "Sliding mode control for systems with mismatched time-varying uncertainties via a self-learning disturbance observer," *Transactions of the Institute of Measurement and Control*, vol. 41, no. 6, pp. 2039–2052, 2018.

[29] Z. Jia, J. Yu, Y. Mei, Y. Chen, Y. Shen, and X. Ai, "Integral backstepping sliding mode control for quadrotor helicopter under external uncertain disturbances," *Aerospace Science and Technology*, vol. 68, pp. 299–307, 2017.

[30] F. Chen, R. Jiang, K. Zhang, B. Jiang, and G. Tao, "Robust backstepping sliding-mode control and observer-based fault estimation for a quadrotor UAV," *IEEE Transactions on Industrial Electronics*, vol. 63, no. 8, pp. 1–5056, 2016.

[31] A. Levant, "Chattering analysis," *IEEE Transactions on Automatic Control*, vol. 55, no. 6, pp. 1380–1389, 2010.

[32] S. Mobayen and J. Ma, "Robust finite-time composite nonlinear feedback control for synchronization of uncertain chaotic systems with nonlinearity and time-delay," *Chaos, Solitons & Fractals*, vol. 114, pp. 46–54, 2018.

[33] S. Mobayen, M. J. Yazdanpanah, and V. J. Majd, "A finite-time tracker for nonholonomic systems using recursive singularity-free FTSM," in *Proceedings of the 2011 American Control Conference*, pp. 1720–1725, San Francisco, CA, USA, 2011.

[34] S. Mobayen, "Design of LMI-based sliding mode controller with an exponential policy for a class of underactuated systems," *Complexity*, vol. 21, no. 5, 124 pages, 2016.

[35] M. Kahouadji, R. Mokhtari, A. Choukchou-Braham, and B. Cherki, "Real-time attitude control of 3 DOF quadrotor UAV using modified super twisting algorithm," *Journal of the Franklin Institute*, vol. 357, no. 5, pp. 2681–2695, 2020.

[36] C. Hua, J. Chen, and X. Guan, "Fractional-order sliding mode control of uncertain QUAVs with time-varying state constraints," *Nonlinear Dynamics*, vol. 95, no. 2, pp. 1347–1360, 2019.

[37] Y. el Houm, A. Abbou, M. Labbadi, and M. Cherkaoui, "Optimal new sliding mode controller combined with modified supertwisting algorithm for a perturbed quadrotor UAV," *International Journal of Aerospace Engineering*, vol. 2020, Article ID 9753870, 10 pages, 2020.

[38] Z. Chu, S. Zhou, M. Zhu, and H. Li, "Finite-time trajectory control for a quadrotor aircraft using disturbance observer," *International Journal of Advanced Robotic Systems*, vol. 17, no. 2, pp. 172988142090384–172988142090311, 2020.

[39] V. K. Tripathi, A. K. Kamath, N. K. Verma, and L. Behera, "Fast terminal sliding mode super twisting controller for position and altitude tracking of the quadrotor," in *2019 International Conference on Robotics and Automation (ICRA)*, pp. 6468–6474, Montreal, QC, Canada, 2019.

[40] N. Wang, Q. Deng, G. Xie, and X. Pan, "Hybrid finite-time trajectory tracking control of a quadrotor," *ISA Transactions*, vol. 90, pp. 278–286, 2019.

[41] Z. Hou, P. Lu, and Z. Tu, "Nonsingular terminal sliding mode control for a quadrotor UAV with a total rotor failure," *Aerospace Science and Technology*, vol. 98, pp. 105716–105718, 2020.

[42] K. Eliker and W. Zhang, "Finite-time adaptive integral backstepping fast terminal sliding mode control application on quadrotor UAV," *International Journal of Control, Automation and Systems*, vol. 18, no. 2, pp. 415–430, 2020.

[43] X. Shao, J. Liu, and H. Wang, "Robust back-stepping output feedback trajectory tracking for quadrotors via extended state observer and sigmoid tracking differentiator," *Mechanical Systems and Signal Processing*, vol. 104, pp. 631–647, 2018.

[44] A. Aboudonia, A. El-Badawy, and R. Rashad, "Active anti-disturbance control of a quadrotor unmanned aerial vehicle using the command-filtering backstepping approach," *Nonlinear Dynamics*, vol. 90, no. 1, pp. 581–597, 2017.

[45] X. Wang and S. Li, "Finite-time consensus for disturbed multi-agent systems with unmeasured states via nonsingular terminal sliding-mode control," in *Advances in Variable Structure Systems and Sliding Mode Control—Theory and Applications*, vol. 115, pp. 269–287, Springer International Publishing, Cham, Switzerland, 2018.

[46] Z. Feng, W. Liang, J. Ling, X. Xiao, K. K. Tan, and T. H. Lee, "Integral terminal sliding-mode-based adaptive integral back-stepping control for precision motion of a piezoelectric ultrasonic motor," *Mechanical Systems and Signal Processing*, vol. 144, article 106856, 2020.

[47] H. Hou, X. Yu, L. Xu, K. Rsetam, and Z. Cao, "Finite-time continuous terminal sliding mode control of servo motor systems," *IEEE Transactions on Industrial Electronics*, vol. 67, no. 7, pp. 5647–5656, 2020.

[48] O. Mechali, L. Xu, Y. Huang, M. Shi, and X. Xie, "Observer-based fixed-time continuous nonsingular terminal sliding mode control of quadrotor aircraft under uncertainties and disturbances for robust trajectory tracking: theory and experiment," *Control Engineering Practice*, vol. 111, article 104806, 2021.

[49] Y. B. Shtessel, I. A. Shkolnikov, and A. Levant, "Smooth second-order sliding modes: missile guidance application," *Automatica*, vol. 43, no. 8, pp. 1470–1476, 2007.

[50] B. Tian, H. Lu, Z. Zuo, and H. Wang, "Fixed-time stabilization of high-order integrator systems with mismatched disturbances," *Nonlinear Dynamics*, vol. 94, no. 4, pp. 2889–2899, 2018.

[51] J. Zhang, S. Yu, and Y. Yan, "Fixed-time extended state observer-based trajectory tracking and point stabilization control for marine surface vessels with uncertainties and disturbances," *Ocean Engineering*, vol. 186, article 106109, 2019.

[52] Q. Xu, "Continuous integral terminal third-order sliding mode motion control for piezoelectric nanopositioning system," *IEEE/ASME Transactions on Mechatronics*, vol. 22, no. 4, pp. 1828–1838, 2017.

[53] M. Labbadi and M. Cherkaoui, "Robust adaptive nonsingular fast terminal sliding-mode tracking control for an uncertain quadrotor UAV subjected to disturbances," *ISA Transactions*, vol. 99, pp. 290–304, 2020.

[54] A. Castillo, R. Sanz, P. Garcia, W. Qiu, H. Wang, and C. Xu, "Disturbance observer-based quadrotor attitude tracking control for aggressive maneuvers," *Control Engineering Practice*, vol. 82, pp. 14–23, 2019.

[55] N. van Hien, V.-T. Truong, and N.-T. Bui, "An object-oriented systems engineering point of view to develop controllers of quadrotor unmanned aerial vehicles," *International Journal of Aerospace Engineering*, vol. 2020, Article ID 8862864, 17 pages, 2020.

[56] M. Reichhartinger, S. K. Spurgeon, M. Forstinger, and M. Wipfler, "A robust exact differentiator toolbox for Matlab®/Simulink®," *IFAC-PapersOnLine*, vol. 50, no. 1, pp. 1711–1716, 2017.

[57] H. Ríos, R. Falcón, O. A. González, and A. Dzul, "Continuous sliding-mode control strategies for quadrotor robust tracking: real-time application," *IEEE Transactions on Industrial Electronics*, vol. 66, no. 2, pp. 1264–1272, 2019.

[58] K. Guo, J. Jia, X. Yu, L. Guo, and L. Xie, "Multiple observers based anti-disturbance control for a quadrotor UAV against payload and wind disturbances," *Control Engineering Practice*, vol. 102, article 104560, 2020.

[59] E. Kayacan, "Sliding mode learning control of uncertain nonlinear systems with Lyapunov stability analysis," *Transactions of the Institute of Measurement and Control*, vol. 41, no. 6, pp. 1750–1760, 2018.

[60] A. Aboudonia, A. El-Badawy, and R. Rashad, "Disturbance observer-based feedback linearization control of an unmanned quadrotor helicopter," *Proceedings of the Institution of Mechanical Engineers, Part I: Journal of Systems and Control Engineering*, vol. 230, no. 9, pp. 877–891, 2016.

[61] W. Wu, X. Xie, M. Wei, O. Mechali, and L. Xu, "Planetary rover path planning based on improved A ∗ algorithm," in *International Conference on Intelligent Robotics and Applications (ICIRA)*, Shenyang, China, 2019.

[62] G. V. Raffo, M. G. Ortega, and F. R. Rubio, "An integral predictive/nonlinear Hꝏ control structure for a quadrotor helicopter," *Automatica*, vol. 46, no. 1, pp. 29–39, 2010.